Article

Cell Reports

Glioblastoma-Associated Microglia Reprogramming Is Mediated by Functional Transfer of Extracellular miR-21

Graphical Abstract

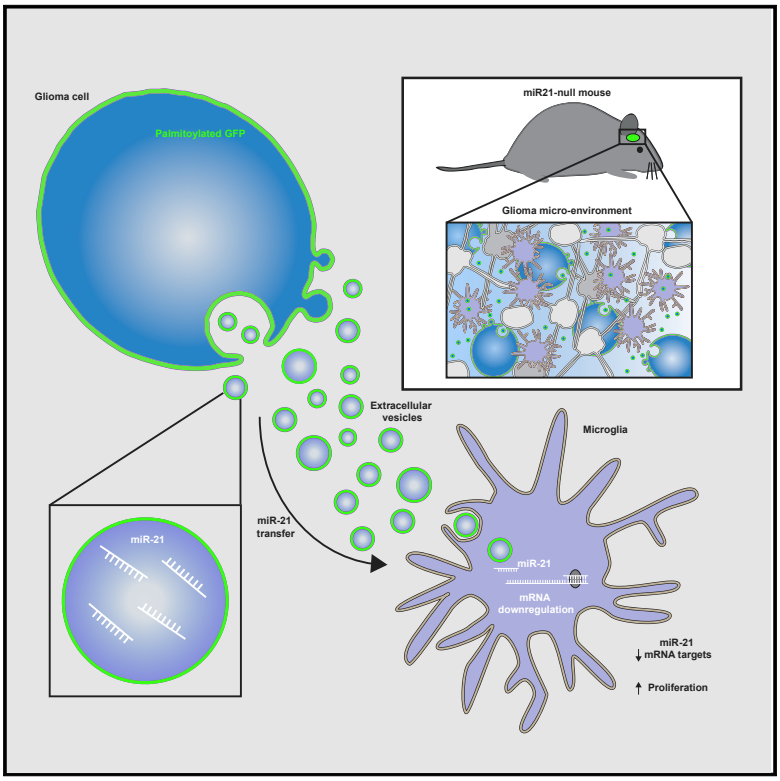

Authors

Erik R. Abels, Sybren L.N. Maas, Lisa Nieland, ..., Anna M. Krichevsky, Marike L.D. Broekman, Xandra O. Breakefield

Correspondence

eabels@mgh.harvard.edu (E.R.A.), breakefield@hms.harvard.edu (X.O.B.)

In Brief

Abels et al. show miR-21 transfer from glioma to microglia by palmitoylated GFP-labeled extracellular vesicles *in vivo*. This transfer results in miR-21 target-specific mRNA downregulation. Following downregulation of *Btg2*, proliferation in microglia is increased, suggesting reprogramming of microglia in the tumor microenvironment through extracellular vesicles shed by glioma cells.

Highlights

- Extracellular vesicles (EVs) shed by glioma cells are taken up by microglia *in vivo*
- miR-21 is functionally transferred from glioma to microglia through EVs *in vivo*
- miR-21 mRNA targets in microglia are downregulated upon EV uptake
- Microglia proliferation is increased after miR-21 target *Btg2* downregulation

Abels et al., 2019, Cell Reports *28*, 3105–3119
September 17, 2019
https://doi.org/10.1016/j.celrep.2019.08.036

CellPress

Cell Reports
Article

Glioblastoma-Associated Microglia Reprogramming Is Mediated by Functional Transfer of Extracellular miR-21

Erik R. Abels,[1,*] Sybren L.N. Maas,[2] Lisa Nieland,[1] Zhiyun Wei,[3] Pike See Cheah,[1,4] Eric Tai,[5] Christy-Joy Kolsteeg,[1] Sophie A. Dusoswa,[6] David T. Ting,[5] Suzanne Hickman,[7] Joseph El Khoury,[7] Anna M. Krichevsky,[3] Marike L.D. Broekman,[8,9,10] and Xandra O. Breakefield[1,10,11,*]

[1]Departments of Neurology and Radiology, Massachusetts General Hospital, and NeuroDiscovery Center, Harvard Medical School, Boston, MA 02129, USA
[2]Department of Neurosurgery, UMC Utrecht Brain Center, University Medical Center, Utrecht University, 3584 CX Utrecht, the Netherlands
[3]Department of Neurology, Ann Romney Center for Neurologic Diseases, Brigham and Women's Hospital, Harvard Medical School, Boston, MA 02115, USA
[4]Department of Human Anatomy, Faculty of Medicine and Health Sciences, Universiti Putra Malaysia, Serdang, Selangor 43400, Malaysia
[5]Cancer Center, Massachusetts General Hospital and Harvard Medical School, Boston, MA 02114, USA
[6]Department of Molecular Cell Biology and Immunology, Amsterdam Infection & Immunology Institute and Cancer Center Amsterdam, Amsterdam UMC, 1081 HZ Amsterdam, the Netherlands
[7]Center for Immunology & Inflammatory Diseases, Massachusetts General Hospital and Harvard Medical School, Boston, MA 02129, USA
[8]Department of Neurosurgery, Leiden University Medical Center, 2300 RC Leiden, the Netherlands
[9]Department of Neurosurgery, Haaglanden Medical Center, 2512 VA The Hague, the Netherlands
[10]Senior author
[11]Lead Contact
*Correspondence: eabels@mgh.harvard.edu (E.R.A.), breakefield@hms.harvard.edu (X.O.B.)
https://doi.org/10.1016/j.celrep.2019.08.036

SUMMARY

Gliomas are primary, diffusely infiltrating brain tumors. Microglia are innate immune cells in the CNS and make up a substantial portion of the tumor mass. Glioma cells shape their microenvironment, communicating with and reprogramming surrounding cells, resulting in enhanced angiogenesis, immune suppression, and remodeling of the extracellular matrix. Glioma cells communicate with microglia, in part by releasing extracellular vesicles (EVs). Mouse glioma cells stably expressing a palmitoylated GFP to label EVs were implanted intracranially into syngeneic miR-21-null mice. Here, we demonstrate functional delivery of miR-21, regulating specific downstream mRNA targets in microglia after uptake of tumor-derived EVs. These findings attest to EV-dependent microRNA delivery as studied in an *in vivo*-based model and provide insight into the reprograming of microglial cells by tumor cells to create a favorable microenvironment for cancer progression.

INTRODUCTION

Gliomas, including glioblastomas (GBs), are the most common and lethal primary adult brain tumors (Ostrom et al., 2013, 2018; Weller et al., 2015). They are characterized and defined by their highly aggressive nature, involving rapid tumor growth, diffuse invasiveness, and resistance to therapy (Stupp et al., 2009). GBs are made up of a heterogeneous population of tumor cells and various types of stromal cells, which all contribute to tumor progression and resistance to treatment (Broekman et al., 2018; Hambardzumyan et al., 2016; Quail and Joyce, 2017). GB cells exert effects on endogenous CNS cell types, such as microglia, astrocytes, oligodendrocytes, endothelial cells, and neurons, as well as infiltrating monocytes and/or macrophages (MOs and/or macrophages) (Broekman et al., 2018; Quail and Joyce, 2017). Among these different cell types, microglia and MOs and/or macrophages are the most prevalent cell types within the tumor (Morantz et al., 1979a, 1979b). Microglia are the resident innate immune cells in the brain (Li and Barres, 2018), whereas MOs residing in a tumor have infiltrated from the blood circulation and can subsequently differentiate to macrophages (Bowman et al., 2016). In response to tumor stimuli, these non-tumorigenic cells produce chemokines and cytokines, including growth and angiogenic factors, immunosuppressive molecules, and extracellular matrix-modifying enzymes, which make the environs favorable to tumor progression (Hambardzumyan et al., 2016; Li and Graeber, 2012).

In addition to soluble factors, GB cells communicate with surrounding cells by release of membrane-bound extracellular vesicles (EVs) containing proteins, lipids, and RNA (Maas et al., 2017). Different RNA species are found in their EVs, including microRNA (miRNA), small nucleolar RNA, Y RNA, mitochondrial RNA, and vault RNA, as well as long non-coding RNA and mRNA (Nolte-'t Hoen et al., 2012; Wei et al., 2017b). EVs are known to carry specific RNA cargo from donor cells to recipient cells (Skog et al., 2008; Valadi et al., 2007). Because the lipid bilayer of the EVs protects the cargo from degradation, EV contents can be delivered to closely surrounding cells as

well as distant recipient cells. Increasing evidence suggests that content can be loaded selectively into EVs (e.g., RNA) (Mateescu et al., 2017) and, once transferred, affect the phenotype of recipient cells, as studied *in vitro* (de Vrij et al., 2015; Skog et al., 2008; Tkach and Théry, 2016; Valadi et al., 2007; van der Vos et al., 2016).

miRNAs are small RNAs, involved in the target cleavage, translational repression, and deadenylation of mRNA (Winter et al., 2009). Among them, miRNA-21 (miR-21) is the most studied in the context of cancer generally and in glioma specifically. The promoter and mature miRNA sequence for miR-21 is highly conserved across a number of vertebrate species (Krichevsky and Gabriely, 2009), with the transcription of miR-21 regulated through an independent promoter site located in the intron region of a protein-coding gene (Fujita et al., 2008). miR-21 has been shown to play a role in embryogenesis, self-renewal, and development in normal cell physiology, but its expression is dysregulated in the context of oncogenic processes (Kumarswamy et al., 2011; Põlajeva et al., 2012). Furthermore, miR-21 expression is associated with cell differentiation and depending on the model system is shown to induce osteogenic differentiation and inhibit neural stem cell differentiation (Gao et al., 2016; Wei et al., 2017a). In GB it has been shown that miR-21 acts as an important oncogene (Chan et al., 2005; Krichevsky and Gabriely, 2009) as high levels of miR-21 in GB lead to the downregulation of the tumor suppressor gene IGFBP3 (Yang et al., 2014) and are associated with activation of metalloproteinases (Gabriely et al., 2008). The expression level of miR-21 is inversely correlated with the survival rate of GB patients (Yang et al., 2014). miR-21 has been identified as a cerebrospinal fluid (CSF) biomarker for monitoring glioma growth and therapy response (Teplyuk et al., 2012). In addition, studies evaluating GB-derived EVs in CSF indicated that elevated miR-21 levels are associated with worse prognosis (Akers et al., 2013; Shi et al., 2015). Interference with miR-21 reduces the malignant potential, as downregulation of miR-21 has been shown to inhibit cell proliferation and invasion *in vitro* and tumor progression *in vivo* (Belter et al., 2016; Corsten et al., 2007; Gabriely et al., 2008; Põlajeva et al., 2012).

In this study we investigated the transfer of miRNA by glioma EVs between tumor and stromal cells using miR-21 as the model miRNA. Using a mouse glioma cell line, GL261, stably expressing a palmitoylated fluorescent protein, we monitored the uptake of EVs by microglia and MOs and/or macrophages in the brain (Lai et al., 2015; van der Vos et al., 2016). To avoid interference by endogenous recipient cell miR-21, GL261 cells were implanted in the brains of mice lacking expression of miR-21 (Ma et al., 2011). Using this reporter we were able to study the uptake of naturally shed EV in an *in vivo* setting. This approach avoids many of the technical issues hampering EV research, such as mechanical manipulation, subselecting for specific EV populations during isolation, and the injection or incubation with an arbitrary number of EVs (Abels et al., 2019; Théry et al., 2018).

Here we demonstrate functional delivery of miR-21 from glioma cells to the surrounding innate immune cells subsequently leading to downregulation of specific miR-21 mRNA targets. Additionally, injection experiments using isolated glioma-derived EVs confirm that the observed effects can be mediated by EVs, although we do not exclude additional involvement of other miR-21 carriers, such as large EV or non-floating non-EV components. Taken together this proves functional EV-mediated miRNA transfer *in vivo* using spontaneously released EVs resulting in reprogramming of microglia.

RESULTS

GL261-Derived EVs Contain High Levels of miR-21

To study the functional extracellular transfer of miRNAs from tumor to surrounding cells *in vivo*, we use syngeneic mouse glioma cells, GL261.palmGFP.H2B.mRFP (GL261.pGHR) (Figure 1A). GL261 cells expressing a palmitoylated form of GFP facilitate tracking of the uptake of tumor-derived membrane fragments, including EVs, into stromal cells in the tumor microenvironment (Lai et al., 2015; van der Vos et al., 2016). In addition, the nuclear localized RFP fused to the H2B histone helps discriminate EV uptake from phagocytosis of whole cells (Welm et al., 2008). Using differential ultracentrifugation (Figure 1B), larger vesicles and cell fragments pelleted at 2,000 × *g*, EVs, including exosomes and microvesicles, isolated from GL261 cell conditioned medium by centrifugation at 100,000 × *g*. Heterogeneity of these different fractions was confirmed by probing for different vesicular protein markers that are present in all types of EVs and larger vesicle fractions (Flotillin-1) (Kowal et al., 2016), those typically associated with exosomes and absent in 2,000 × *g* (ALIX and TSG101), and GAPDH found to be enriched in the 2,000 × *g* and cellular fraction (McNamara et al., 2018). Importantly, GFP protein was detected in both cellular and extracellular fractions, confirming that this marker can be used to track the fate of all different subtypes of EVs (Figure 1C). Nanoparticle tracking analysis (NTA) of the EVs isolated by 100,000 × *g* ultracentrifugation revealed a broad size distribution of EVs ranging from 100 to 500 nm, further confirming their heterogeneity (Figure S1A). Importantly, miR-21 was present in GL261 cells, 2,000 × *g* fraction, and GL261-derived EVs, with significantly higher levels of miR-21 in the EVs compared with cellular levels (Figures 1D and 1E). The level of miR-21 in cells, the 2,000 × *g* fraction, and EVs was higher than the level of to the miR-10b, a miRNA uniquely expressed in glioma (El Fatimy et al., 2017), compared with normal brain (Figures S1B and S1C). To further confirm the presence of miR-21 in EVs, we separated the different-sized vesicles collected at 100,000 × *g* and performed an iodixanol gradient. The EVs were bottom-loaded, and the gradient was performed over 16 h at 156,000 × *g* (Figure S2A). In total, 12 fractions were collected and analyzed for GFP protein levels, as well as miR-21 levels. Overall, miR-21 was found to co-localize with GFP, but miR-21 was also present in the high-density fractions, possibly associated with high-density lipoproteins (Figures S2B and S2C) (Vickers et al., 2011). Taken together, the heterogeneous population of EVs shed by tumor cells is labeled with membrane-bound GFP and contains high levels of miR-21.

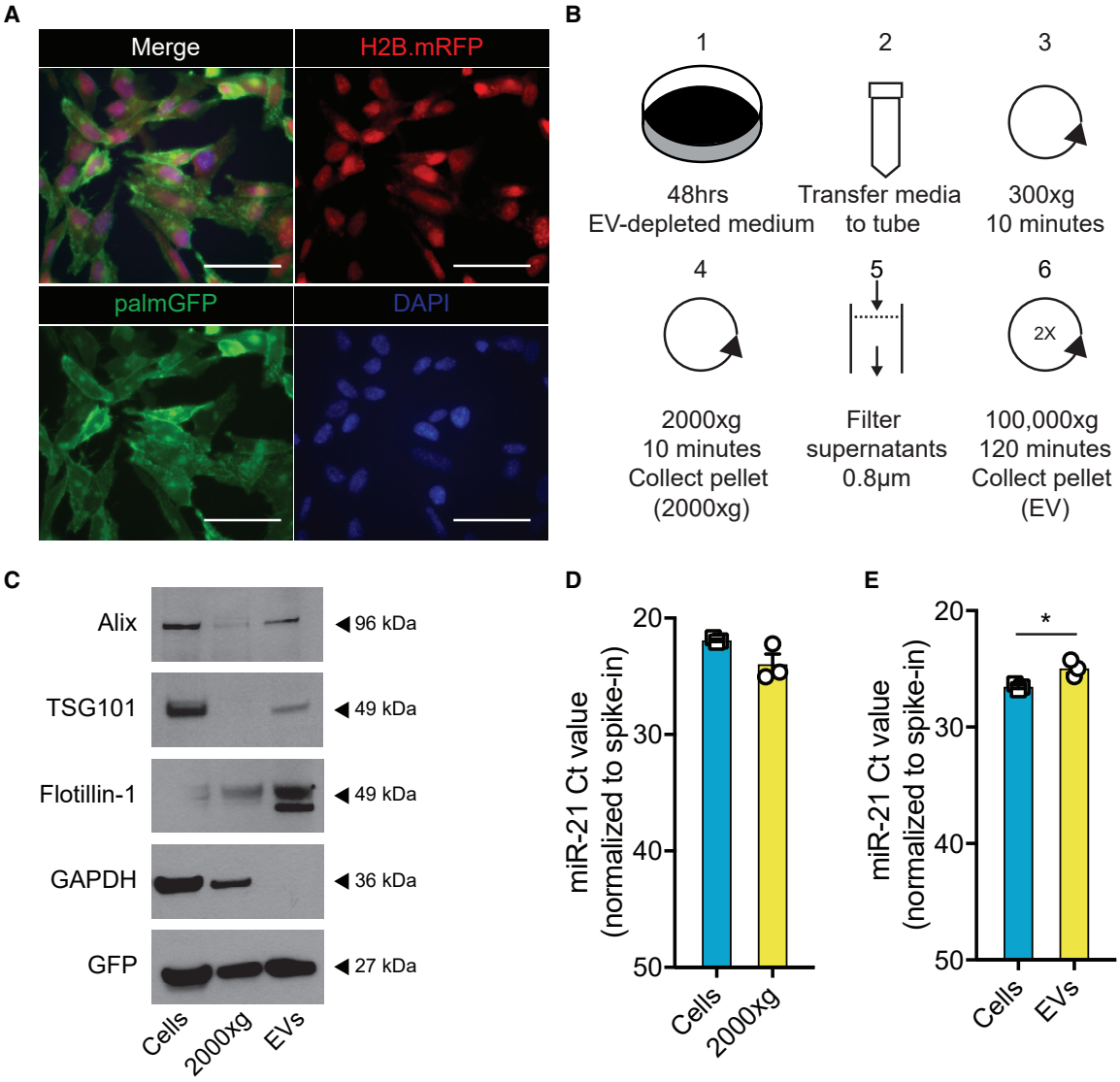

Figure 1. miR-21 Is Abundantly Present in GL261 Tumor Cells and Isolated EVs

(A) GL261 cells were transduced to stably express palmitoylated GFP (palmGFP; lower left panel) as a membrane marker and the H2B.mRFP (upper right panel) as a nuclear marker that co-localized with DAPI (lower right panel). Scale bar, 50 μm.

(B) Schematic overview of EV isolation using differential centrifugation. Pellets acquired after first round of ultracentrifugation were concentrated by second round of ultracentrifugation to obtain purer population of EVs.

(C) Western blot demonstrates vesicle markers (ALIX and Flotillin-1) excluding TSG101, enriched in EV lysates. GFP was detected in all lysates (equal protein amount loaded).

(D) Expression level of miR-21 analyzed using qRT-PCR, as plotted in Ct value normalized to spike-in (UniSp6), shows similar levels of miR-21 in cells and 2000 × *g* fraction.

(E) Expression level of miR-21 analyzed using qRT-PCR, as plotted in Ct value normalized to spike-in (UniSp6), shows higher levels of miR-21 in EVs compared with cells.

Data represent three independent experiments and are presented as the mean with SEM (error bars). $p < 0.05$, unpaired t test.

Tumor-Derived EVs Effectively Deliver miR-21 to Microglia

Next, GL261.pGHR cells or carrier fluids were injected in adult miR-21-null mouse brains. By using miR-21-null mice, we were able to differentiate between endogenous upregulation of miRNAs following tumor implantation and the transfer of exogenous miR-21 from the tumor to stromal cells. In this model, endogenous miR-21 is not expressed in stromal cells, so the presence of miR-21 should be derived exclusively from the implanted tumor cells. Three weeks after implantation, mice were euthanized, and brains were mechanically and enzymatically digested for subsequent fluorescence-activated cell sorting (FACS) (Figure 2A). Microglial cells were sorted on the basis of the absence of RFP (black gate) and levels of

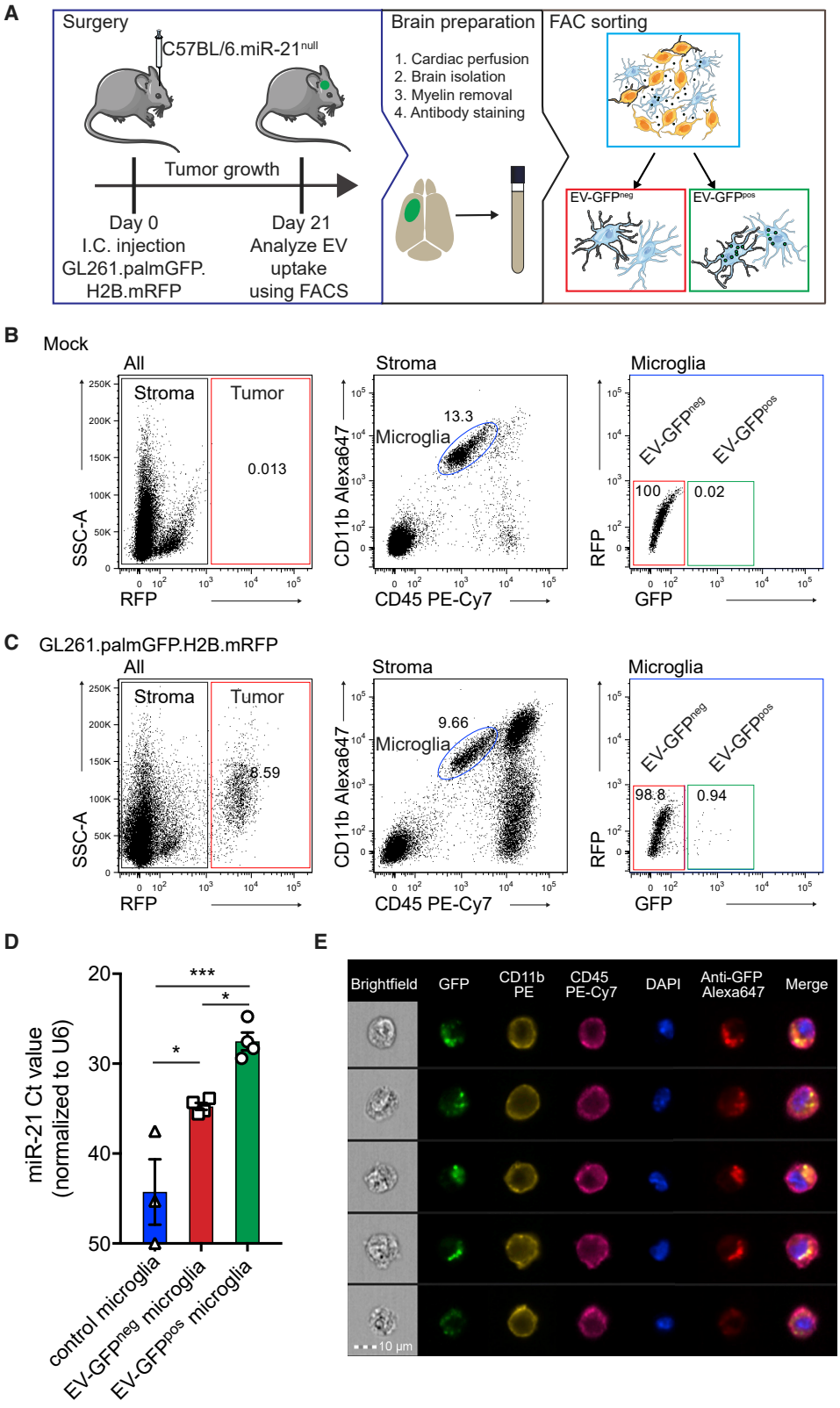

(legend on next page)

CD11b and CD45 (blue gate) (Bennett et al., 2016). A carrier fluid-injected (mock) brain was used to determine the GFP cut-off (red and green gate) (Figure 2B). From tumor-bearing brain, microglial cells were isolated with the control GFP cut-off used to separate cells negative for GFP (red box; EV-GFP^{neg}) and positive for GFP (green box; EV-GFP^{pos}). The presence of GFP in microglia thus indicates tumor-derived EV uptake (Figure 2C). The expression level of miR-21 was detected at significantly higher levels in microglia, which had taken up tumor EVs compared with GFP-negative cells (Figure 2D). The difference detected between mock microglia and EV-GFP^{neg} microglia could be due to uptake of high-density lipoproteins, which carry some miR-21 (Figure S2). A similar trend between EV-GFP^{neg} and EV-GFP^{pos} microglia was seen in glioma-specific miR-10b, in which the expression level was higher than in EV-GFP^{neg} microglia (Figure S1D). Using a similar approach, MOs and/or macrophages were identified by their high expression of CD45 and CD11b (blue gate, as indicated in the figure legend) (Bennett et al., 2016), separating GFP-positive cells from GFP-negative cells (Figures 3A and 3B). Similar to the microglial cells, an increased level of miR-21 was detected in EV-GFP^{pos} MOs and/or macrophages in comparison with EV-GFP^{neg} cells (Figure 3C). Surprisingly the difference between EV-GFP^{neg} and GFP^{pos} in MOs and/or macrophages was smaller, and the relative levels in EV-GFP^{pos} MOs and/or macrophages were lower compared with EV-GFP^{pos} microglia (Figures 2D and 3C). To further validate that the GFP uptake is caused by EV-sized particles rather than phagocytosis of complete cells, ImageStream analysis was used to visualize the uptake of GFP in microglial cells and MOs and/or macrophages (CD11b-PE, CD45-PE-Cy7 positive), using anti-GFP conjugated with Alexa Fluor 647 to exclude auto-fluorescence frequently encountered in myeloid cells and to confirm the uptake of GFP^{pos} vesicle-like structures (Figures 2E and 3D). This analysis, as expected, did confirm the presence of subcellular GFP-positive particles in the microglial cells and MOs and/or macrophages cells (Figures 2E and 3D). To confirm if the transfer of GFP is associated with functional miR-21 transfers into microglia, the miR-21 levels in cells after EV uptake were examined (Figure 2D). To further investigate to what extend EVs are taken up by other immune cells, we quantified GFP uptake by CD11b^{low}CD45^{high} lymphocytes (Figure S3A). In this population of non-phagocytic cells, we found a smaller percentage of cells that have taken up EV-GFP (Figures S3A and S3B). Moreover, the ImageStream and FACS analysis also allowed us to verify the expression of CD11b and CD45 on microglia and the absent of expression in tumor cells (Figures S4A–S4D). Taken together, this demonstrates that the combination of CD11b and CD45 can be used to isolate microglia and MOs and/or macrophages cells and that GFP-positive EVs released by tumor cells *in vivo* can transfer miR-21 to microglia.

EV-Mediated Transfer of miR-21 Leads to Downregulation of Specific mRNA Targets in Microglia

One of the main functions of miR-21 is mRNA target cleavage, leading to reduction of levels of specific mRNAs. To study this, we analyzed the mRNA transcriptome of microglia, which were separated by FACS on the basis of whether they contained EV-GFP. Unsupervised clustering of the top 750 most differentially expressed genes showed a clear distinction between microglia from control and tumor-bearing EV-GFP^{neg} and EV-GFP^{pos} microglia (Figure 4A). To focus on the effect of the miR-21 transfer from tumor cells to microglia, the transcripts in EV-GFP^{neg} and EV-GFP^{pos} microglia were further analyzed. Four hundred forty-one genes were significantly upregulated and 359 genes were downregulated in EV-GFP^{neg} versus EV-GFP^{pos} (Figure 4B, significantly changed genes in red). To further investigate miR-21 targets, we derived a list of miR-21 targets by merging the results from two publicly available databases (miRTarBase and miRWalk) (Chou et al., 2018; Dweep and Gretz, 2015; Dweep et al., 2011); all references and evidence to miR-21 targets listed in the database were manually curated. To focus on validated targets rather than predicted targets, only genes from references showing direct downregulation of target genes on the basis of luciferase assays, qPCR analyses, or western blots were included (Table S1). Relative gene expression of the selected 59 target genes showed 25 genes with lowest expression in EV-GFP^{pos} microglia (Figure 4C). The genes with significantly reduced expression in the EV-GFP^{pos} compared with EV-GFP^{neg} microglia (adjusted p [p-adj] < 0.05) include *Nfat5*, *Bmpr2*, *Btg2*, *Rhob*, and *Kbtbd2* (Figure 4C, significantly changed genes in bold). Interestingly, two genes (*FasL* and *Tgfbi*) regulated by miR-21 are expressed at a significantly higher level in EV-GFP^{pos} compared with EV-GFP^{neg} microglia (p-adj < 0.05) (Figure 4C). Overall, these results demonstrate that the transfer of miR-21 by EVs *in vivo* results in downregulation of some of the miR-21 target mRNAs.

Figure 2. miR-21 Is Transferred to Microglia after Uptake of Tumor-Derived EVs

(A) Schematic illustration of experimental setup using C57BL/6.miR-21-null mice implanted with GL261.palmGFP.H2B.mRFP glioma cells that release palmGFP fluorescent EVs. Brains were harvested 21 days after implantation. Tissue was dissociated using enzymatic and mechanic digestion and microglia sorted on the basis of cell markers and EV-GFP uptake.

(B) Representative FACS plots showing gating strategy in which RFP expression is used to exclude tumor cells in downstream analysis, and subsequently microglia were identified as CD11b^{high}/CD45^{med} cells (blue gate). Microglia were then sorted on the basis of the GFP signal, detected as the upper limit in control (no tumor).

(C) In mice implanted with GL261.palmGFP.H2B.mRFP, similar analysis (as in B) revealed a population of GFP-positive microglia (green gate in the microglia plot).

(D) Uptake of EV-GFP results in the elevated levels of miR-21 in microglia, compared with control microglia (blue), with Ct > 40 considered baseline.

(E) EV-GFP uptake visualized by imaging flow cytometry using ImageStream. Five representative cells presented showing EV-GFP co-localized with anti-GFP Alexa Fluor 647 within the contours of microglia as show by membrane marker CD11B and CD45. Scale bar, 10 μm.

Data represent four independent experiments and are presented as the mean with SEM (error bars). *p < 0.05 and **p < 0.01, one-way ANOVA with Tukey's multiple-comparisons test.

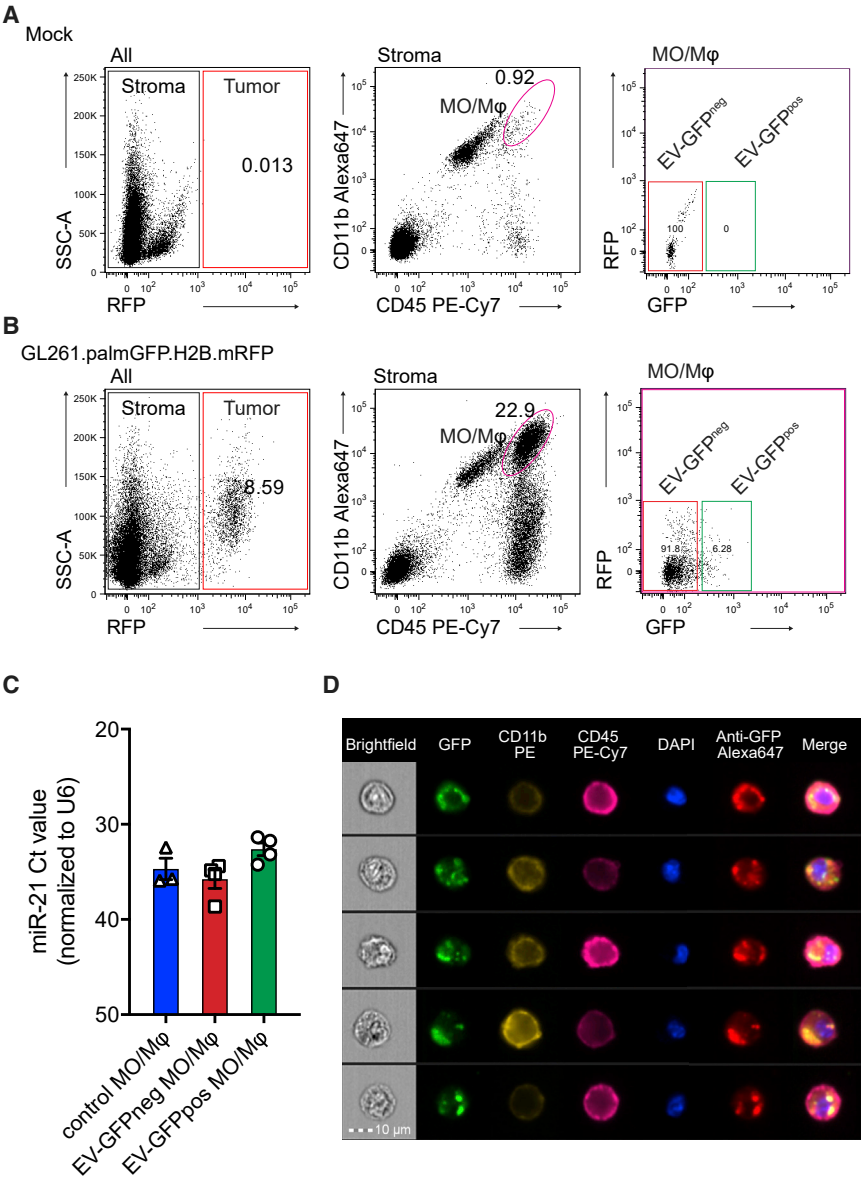

Figure 3. miR-21 Is Transferred to Monocytes and/or Macrophages after Uptake of Tumor-Derived EVs

(A) Monocytes and/or macrophages (MOs and/or macrophages) from miR-21-null mice were identified by FACS as CD11b^{high}/CD45^{high} cells (magenta gate). MOs and/or macrophages were then sorted on the basis of the GFP signal detected as the upper limit in control (no tumor).

(B) In mice implanted with GL261.palmGFP.H2B.mRFP, a population of GFP-positive MOs and/or macrophages was identified (green gate in the GFP/RFP plot).

(C) Uptake of EV-GFP resulted in the presence of miR-21 in MOs and/or macrophages.

(D) EV-GFP uptake was visualized by imaging flow cytometry using ImageStream. Scale bar, 10 μm.

Data represent three independent experiments and are presented as the mean with SEM (error bars). One-way ANOVA with Tukey's multiple-comparisons test.

miR-21 Downregulates Genes Involved in Cell Proliferation in Microglia

Although the selected mRNA targets (Figure 4C), which are targets of miR-21 (Table S1), are found in a variety of cell types, we set out to validate these targets in microglia *in vitro*. Cultures of primary microglia isolated from neonatal miR-21-null mice were transfected with a miR-21 mimic and a scrambled control RNA. Subsequently, the levels of the mRNA targets identified in the *in vivo* setting were tested using qRT-PCR. From the selected genes, expression levels for *Btg2* and *Nfat5* as well as *Pdcd4* were significantly downregulated after EV uptake *in vivo* and were shown to be significantly downregulated by the miR-21 mimic (Figure 5A). A control gene not targeted by miR-21, *Gapdh*, was not affected, an indication that mRNA target gene downregulation is miR-21 specific (Figure 5B). In order to evaluate the effects of transfer of miR-21 by tumor-derived EVs to microglia *in vitro*, EVs from conditioned media (EV) and unconditioned media (UcM) (from cultures with and without GL261 cells, respectively) were isolated using a differential centrifugation protocol (Figure 5C). Primary neonatal miR-21-null mouse microglia were then incubated with EVs and UcM. The microglia, 1 × 10^5 cells, were exposed to a single dose of EVs, 2.43 × 10^{10} particles. Twenty-four hours later, the expression level of miR-21 was significantly increased in microglia exposed to GL261-derived EVs, compared with UcM (Figure 5D). We also observed significant downregulation of the *in vivo* EV downregulated miR-21 targets *Bmpr2*, *Btg2*, *Kbtbd2*, *Pdcd4*, *Pten*, and *Rhob* transcripts, while *Gapdh* expression appeared unaffected (Figures 5E and 5F). Also, we tested whether microglia from wild-type mice were also affected by the uptake of glioma-derived EV in a similar way. We exposed primary neonatal wild-type microglia to a single dose of EVs (2.43 × 10^{10} particles). Expression levels of the miR-21 targets were analyzed 24 h after EV exposure. Here we found similar trends of downregulation of the mRNA targets (Figure S5A). Using a similar approach as shown in Figure 2, we isolated microglia from a tumor-bearing brain of a miR-21-expressing mouse and investigated the levels of miR-21 targets. We found similar patterns of downregulation of miR-21 targets in the miR-21 wild-type mice compared with miR-21-null mice (Table S1; Figure S5B). Taken together, these data demonstrate that miR-21, either introduced by transfection or delivered through EVs, can downregulate specific mRNAs in miR-21-null and wild-type microglia that were downregulated *in vitro* and *in vivo*.

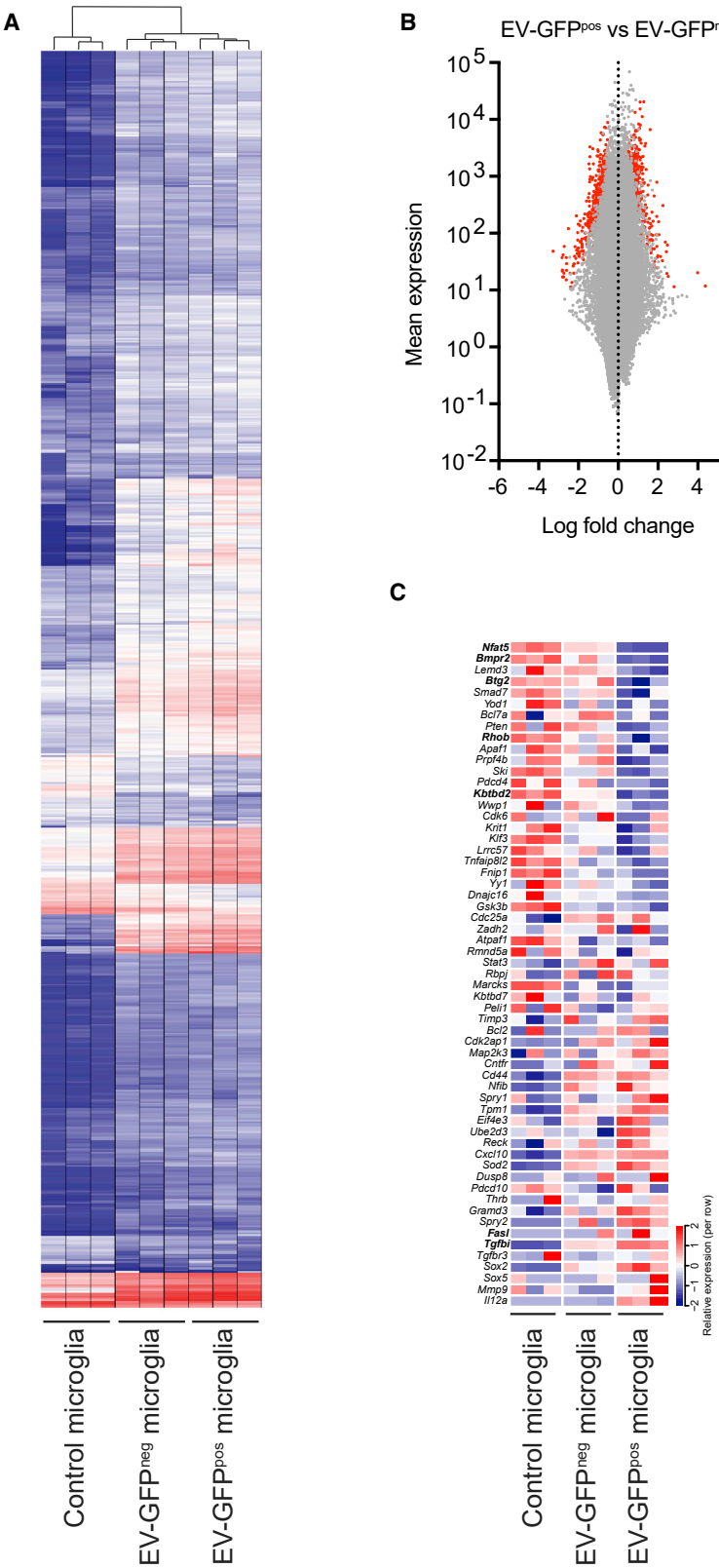

Figure 4. miR-21 Downregulates Target mRNAs in Tumor-Associated Microglia

(A) In unsupervised clustering analysis, the top 750 most differentially expressed genes microglia clustered on the basis of tumor status and EV-GFP uptake status.

(B) MA-plot shows 441 significantly upregulated and 359 downregulated genes (plotted in red) when comparing EV-GFP^{pos} with EV-GFP^{neg} microglia.

(C) Heatmap shows relative gene expression for 59 validated miR-21 gene targets. Bold gene names indicate genes with p-adj < 0.05 in differential expression analysis EV-GFP^{pos} versus EV-GFP^{neg} microglia.

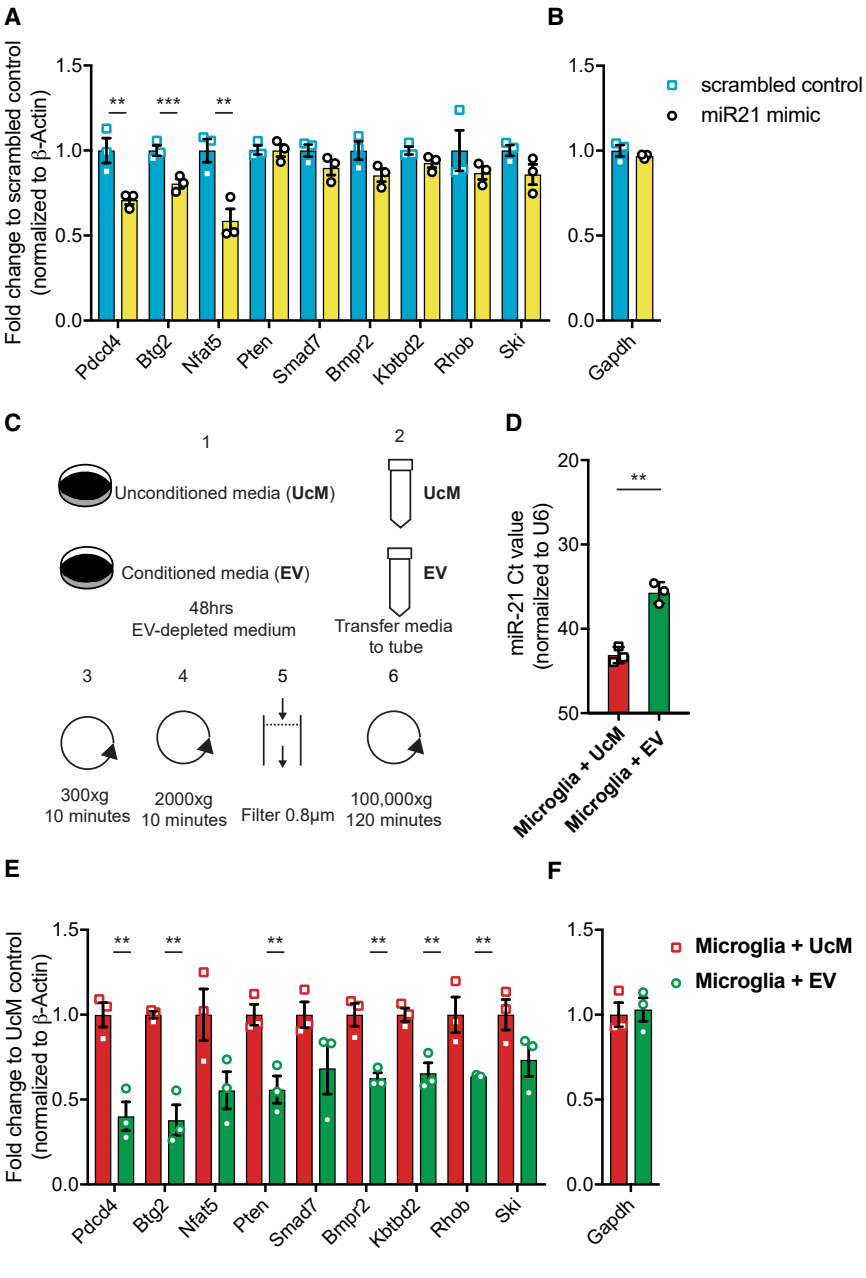

Figure 5. miR-21 Regulates Selected Target Genes *In Vitro* in Primary Neonatal Microglia

(A) In comparison with scrambled control, transfection of miR-21-mimic in primary neonatal miR-21-null mice microglia results in significant downregulation of miR-21 target genes (*Btg2*, *Nfat5*, and *Pcdc4*) normalized to *β-Actin*.

(B) Transfection of miR-21-mimic in primary neonatal miR-21-null mice microglia did not affect a control gene *Gaphd* (not targeted by miR-21).

(C) Schematic overview of EV isolation using differential centrifugation. EVs from conditioned media cultured with GL261 cells (EV) and unconditioned media (UcM) were subjected to differential centrifugation. Collected EV pellet was resuspended in PBS and added to miR-21-null microglia.

(D) EVs from conditioned media (EV) and unconditioned media (UcM) were isolated and added to miR-21-null primary microglia followed by 24 h incubation. Increased levels of miR-21 were detected in microglia exposed to GL261-derived EV, compared with control media, with Ct > 40 considered baseline.

(E and F) Fold expression of miR-21 target genes (*Bmpr2*, *Btg2*, *Kbtbd2*, *Nfat5*, *Pdcd4*, *Pten*, *Rhob*, *Smad7*, and *Ski*) (E) and (F) *Gapdh*, a gene not targeted by miR-21, normalized to *β-Actin* in miR-21-null microglia exposed to GL261-derived EVs, compared with UcM.

Data represent three independent experiments and are presented as the mean with SEM (error bars). **p < 0.01 and ***p < 0.001, unpaired t test and multiple t test.

Intracranial Delivery of GL261-Derived EVs Results in Effective Transfer of miR-21 in Endogenous Cells

Our *in vitro* experiment showed that EV-mediated miR-21 transfer downregulates a select number of target mRNAs in microglia, hence it is important to evaluate whether this effect also occurs in an *in vivo* setting. By using EVs isolated from GL261, grown *in vitro*, we can study the uptake and effect of these EVs without confounding action of other factors released by the tumor cells. Using the previously described 100,000 × *g* EV isolation protocol (Figure 1B), we resuspended the GL261-derived EVs in PBS. A total of 1.26 × 10^9 particles as measured by NTA were used. A carrier control (PBS) was used to set the cut-off of the GFP within the microglial population (blue circle and green box) (Figure 6A). Sixteen hours after injection of the EVs into the left striatum (using similar coordinates as tumor implantation) of miR-21-null mice, about 0.3% of all microglia in the brain (blue circle) that had taken up EVs (green box) were detected (Figure 6B). Interestingly, miR-21 was detected in the EV-GFP^{pos} microglia, compared with being at non-detectable levels in EV-GFP^{neg} microglia, demonstrating that miR-21 was effectively transferred via EVs derived from *in vitro* cultured tumor cells and delivered to microglia *in vivo* (Figure 6C). This EV uptake occurs soon after injection, as the EV-GFP signal was no longer detectable 40 h after injection of EVs (data not shown), indicating the degradation of EV-GFP. *In vitro* experiments showed that levels of *Pdcd4* and *Btg2* were regulated by miR-21 in microglia (Figure 5A) and were shown to be downregulated after exposure to glioma EVs (Figure 5D). In this experiment, both transcript levels were reduced in microglia that took up EV-GFP, but this reduction reached significance only for the *Btg2* replicates (Figure 6D). Interestingly, of the two targets, only *Btg2* was among the initially downregulated miR-21 targets *in vivo*. The levels of miR-21 were lower in the microglia after EV-GFP uptake (delivered intracranially), compared with the

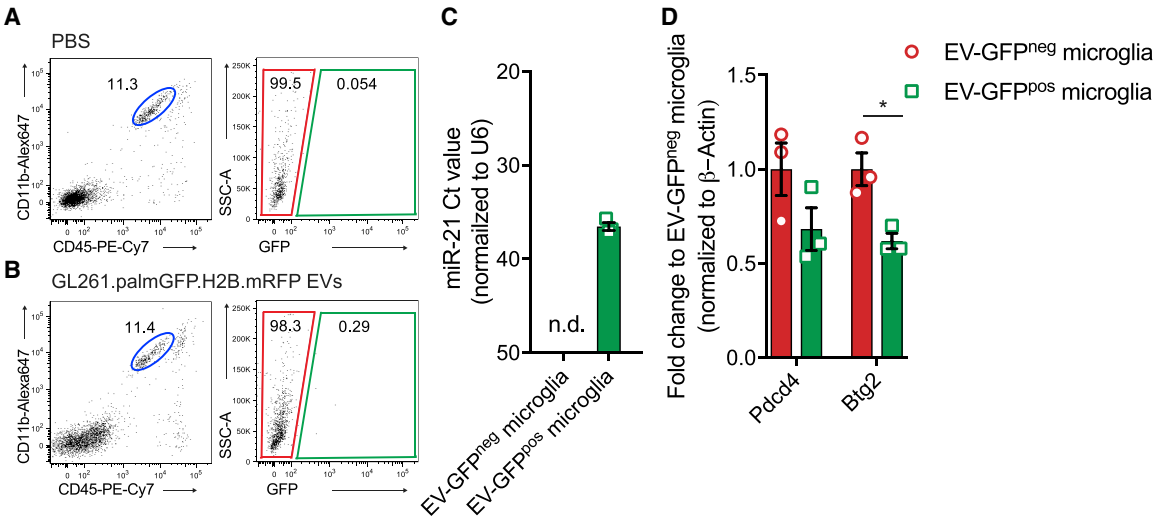

Figure 6. EV-GFP Uptake after EV Intracranial Injection

(A and B) PBS (A) or GL261.palmGFP.H2B.mRFP (B) EVs were injected intracranially. After 16 h brains were dissociated and microglia were sorted on the basis of EV-GFP uptake.

(C) Uptake of EV-GFP resulted in elevated levels of miR-21 in microglia; levels in EV-GFP^{neg} microglia were not detectable (n.d.), with Ct > 40 considered baseline.

(D) Gene expression analyzed using ddPCR showing that *Pdcd4* and *Btg2* expression is reduced after EV-GFP uptake.

Data represent three independent experiments and are presented as the mean with SEM (error bars). *p < 0.05, multiple t test.

tumor samples or microglia transfected *in vitro*. The relatively low levels of miR-21 in the EV-GFP brain injection experiment may explain the incomplete downregulation of the *Pdcd4* gene. However, these results suggest that in the absence of a tumor, microglia can take up tumor cell-derived EVs injected into the striatum, leading to miR-21-dependent downregulation of *Btg2*.

Btg2 Downregulation Leads to Increased Microglia Proliferation

A number of the downregulated genes, including *Pdcd4* and *Btg2*, are involved in cellular proliferation. Pathway analysis of genes differentially expressed at higher levels in EV-GFP^{pos} compared with EV-GFP^{neg} microglia indeed showed that a number of pathways involved in cell cycle control were upregulated, indicating a higher degree of proliferation in microglia after EV uptake (Figure S6A). To test whether microglia have a higher degree of proliferation after EV uptake, we analyzed the expression level of a number of genes that are described to be involved in microglial proliferation (Hammond et al., 2019). All of these genes are expressed at higher levels in microglia from tumor-bearing brains, with the highest expression in EV-GFP^{pos} microglia (Figure 7A). To further investigate the effect of miR-21 and *Btg2* on microglial proliferation, we transfected miR-21-knockout (KO) microglia with miR-21 mimic or small interfering RNA (siRNA) against *Btg2*. Thereafter, the number of Ki67-positive cells was quantified comparing miR-21 mimic versus scrambled control and siRNA targeting *Btg2* versus a siRNA control. Using a miR-21 mimic, a larger number of microglia express the Ki67 proliferation marker after 24 h of transfection (Figures 7B and 7C). The downregulation of *Btg2* after siRNA transfection also yielded a larger number of microglia expressing Ki67 (Figures 7D–7F). Overall, these results show that microglial proliferation is increased upon the delivery of miR-21 and after the downregulation of *Btg2*.

DISCUSSION

EV-mediated miRNA transfer downregulates specific mRNAs *in vivo*. By using a palmitoylated fluorescent protein stably expressed in tumor cells, we were able to track the uptake of tumor EVs by other cells in the brain (Lai et al., 2015; van der Vos et al., 2016). This reporter is not specific to one type of vesicles (e.g., exosomes, ectosomes, or microvesicles) (Cocucci and Meldolesi, 2015) but follows the uptake of all naturally formed membrane-bound vesicles. Microglia are known to be highly infiltrative into gliomas, and we have shown that they avidly take up tumor-derived fluorescent EVs (van der Vos et al., 2016). Here we show that the cargo of the EVs is transferred into the microglia, resulting in the delivery of functional miR-21.

In the current literature, EVs isolated after ultracentrifugation (100,000 × *g* pellet) or smaller EVs isolated after size exclusion chromatography have been studied the most. We included the 2,000 × *g* pellet (composed mostly of apoptotic bodies) in our analysis as well, and even though we were able to detect miR-21 in these particles, we could not detect upregulation of miR-21 compared with cellular levels, as were found for the 100,000 × *g* pellet. Additionally by injecting the 2,000 × *g* pellet into non-tumor-bearing mice, we detected only incidental GFP uptake by microglia, indicating that the EVs isolated after ultracentrifugation are taken up to a greater extent microglial cells *in vivo*. Moreover, we found that miR-21 is also present in the high-density fractions by density gradient centrifugation (containing high-density lipoproteins), indicating that these may add to the EV-mediated miR-21 transfer and could explain the presence of miR-21 in GFP^{neg} microglia (Vickers et al., 2011).

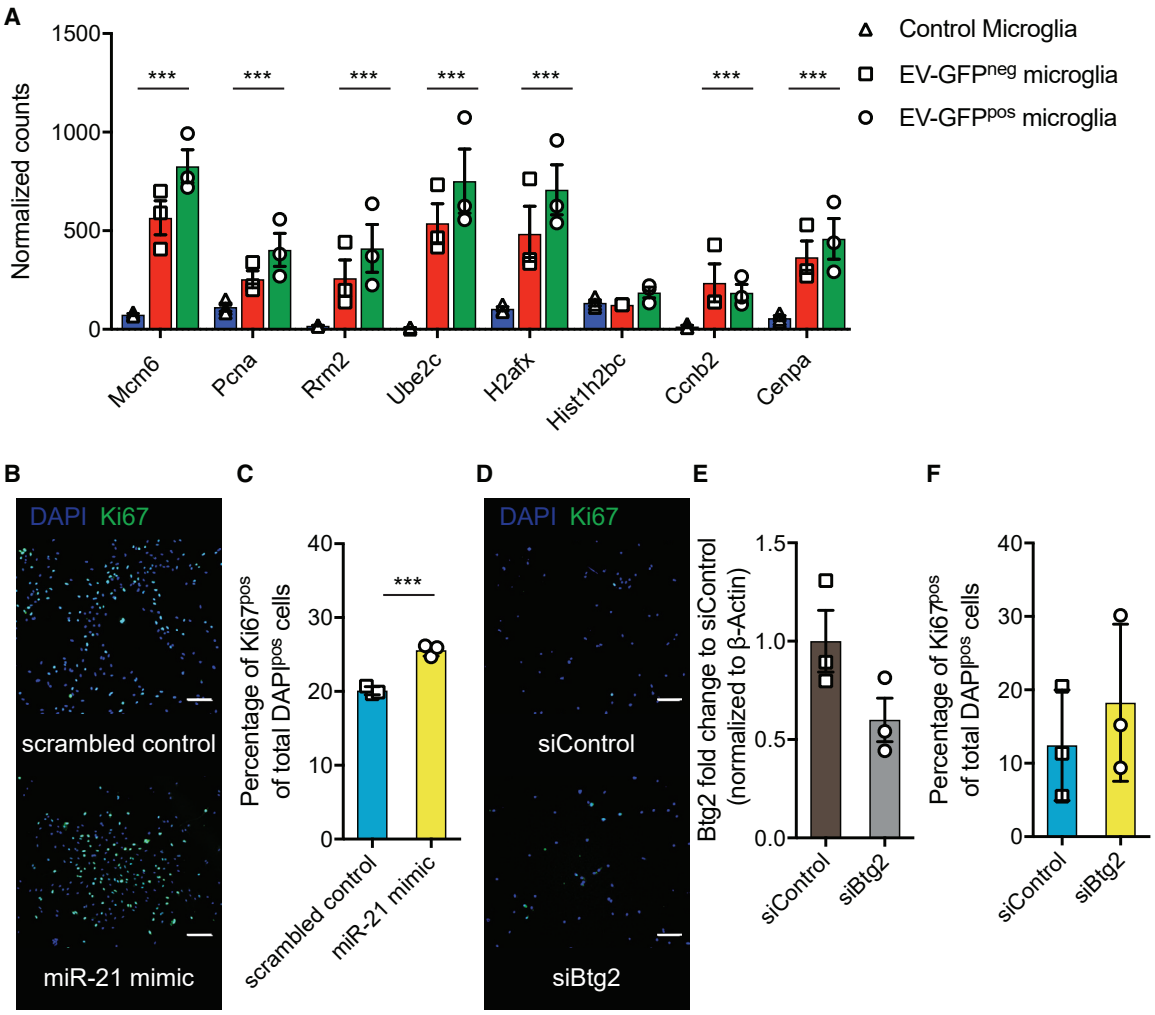

Figure 7. *Btg2* Downregulation Leads to Increased Microglia Proliferation

(A) Normalized read count of genes involved in microglia proliferation (Hammond et al., 2019).

(B) Representative images of *in vitro* culture miR-21-null microglia transfected with miR-21 mimic and control showing DAPI and Ki67 staining 24 h after transfection. Scale bar, 100 μm.

(C) Quantification of proliferation 24 h after transfection with miR-21 mimic or control as measured by Ki67-positive cells per total number of DAPI-positive cells.

(D) Representative images of *in vitro* culture miR-21-null microglia transfected with siRNA against *Btg2* and siRNA control showing DAPI and Ki67 staining 24 h after transfection. Scale bar, 100 μm.

(E) Quantification of proliferation 24 h after transfection with siRNA against *Btg2* or control as measured by Ki67-positive cells per total number of DAPI-positive cells.

Data represent three independent experiments and are presented as the mean with SEM (error bars). ***$p < 0.001$, multiple testing adjusted p value differential expression in (A), and ***$p < 0.001$, unpaired t test in (C), (E), and (F).

Overall, the cargo of the glioma-derived EV subtypes is transferred into the microglia, resulting in the delivery of functional miR-21. Although EV-mediated miRNA transfer was previously either shown *in vitro* or after injection of arbitrary amounts of highly subselected EVs *in vivo*, this study demonstrates *in vivo* functional transfer of miRNA by spontaneously released EVs.

Because of their high abundance in tumor tissue, we focused in this study on the microglia and infiltrating MOs and/or macrophages. Analysis of the EV-GFP uptake and the subsequent miR-21 levels in miR-21-null mice showed that although the percentage of cells positive for EV-GFP uptake was highest in the MO and/or macrophage population, the miR-21 transfer was most efficient in microglia. This could be due to differential uptake mechanisms; for example, microglia have been known to take up EV through macropinocytosis, whereas MOs and/or macrophages use phagocytosis, possibly followed by degradation (Fitzner et al., 2011). These differential uptake mechanisms can result in the difference of miR-21 level detected. So far, it has been reported that EVs derived from oligodendrocytes, glioma cells, and neural stem cells are taken up by microglia (Fitzner et al., 2011; Morton et al., 2018; van der Vos et al., 2016). Within the developing brain, the role of EVs in the

communication between neural stem cells and neighboring microglia has also been shown to change the transcriptional state of the latter (Morton et al., 2018). Here, we used flow cytometry and image flow cytometry to visualize the uptake of fluorescently labeled EVs by microglia. By analyzing the transcriptome of the tumor-associated miR-21-null microglia, we observed downregulation of miR-21 target mRNAs after uptake of tumor EVs. Overall, following uptake of the fluorescent EVs, miR-21 needs to exit the vesicles to become functional. Upon release of miR-21 and palmitoylated GFP (palmGFP) into the cytosol, the palmGFP might associate with other membranes in the cells and would probably be diluted out so as to be lost visually. Alternatively, a fraction of miR-21 and palmGFP might be retained in endosomes and degraded in late endosomes and lysosomes. Because the uptake of palmGFP EVs is most probably not a one-time but a continuous process, palmGFP and thus levels of miR-21 in cells may be in both the endosomes and cytosol and/or membranes. The downregulation of target mRNAs as we detected supports the notion that miR-21 is release into the cytosol after uptake of miR-21^{+} tumor EVs. Although other EV components, such as different small and large RNAs as well as proteins and lipids, are also anticipated to affect microglia, we have, by making use of the miR-21-null mouse, been able to dissect the effects of the transfer of this single miRNA. Especially for *Btg2* we were able to show EV miR-21-mediated knockdown *in vivo* and were able to validate the role of EVs in additional *in vivo* and *in vitro* studies.

Here, we have demonstrated a mechanism through which a tumor can change the molecular profiles of microglia. EV-mediated transfer of miRNA from tumor cells to microglia results in downregulation of specific target genes. The gene that was most strikingly altered by EV-mediated miR-21 transfer was *Btg2* (synonyms, *Pc3* and *Tis21*). This gene belongs to the BTG/Tob protein family, which is composed of six genes (*BTG1*, *BTG2/PC3/Tis21*, *BTG3/ANA*, *BTG4/PC3B*, *Tob1/Tob*, and *Tob2*), and all are involved in the control of cellular proliferation and differentiation (Matsuda et al., 2001). *Btg2* negatively controls proliferation by reducing the activity of cyclin D1, which drives the cell cycle, as shown in medulloblastoma cells (Farioli-Vecchioli et al., 2007), and by inhibiting cell cycle transition from G1 to S phase in fibroblasts (Guardavaccaro et al., 2000). Increased levels of proliferation in microglia have been reported in neuro-inflammation and traumatic brain injury, indicating that disruption of CNS homeostasis as is also occurring during tumor growth can result in proliferation of microglia (Febinger et al., 2015; Pepe et al., 2017). By downregulation of *Btg2* through transfection with miR-21 mimic or siRNA specific to this message, we showed an increased level of proliferation in microglia in culture. Within a tumor it is possible that by reducing the anti-proliferative effects of *Btg2* in tumor-supporting microglia, these cells will increase proliferation, resulting in an increased influence on shaping the tumor microenvironment. In addition, it has also been shown that glioma cells exchange extracellular material, suggesting that EV-mediated miR-21 transfer can also increase glioma cell proliferation (Al-Nedawi et al., 2008; Skog et al., 2008).

In conclusion, the results of this study demonstrate that glioma cells can reprogram microglia in part by transferring miR-21 through EVs. Using the fluorescent palmitoylated EV reporter, we have been able to study the uptake of naturally secreted EVs *in vivo*. Reviewing our data, we propose a model in which EVs secreted by tumor cells function as miRNA carriers, which deliver molecules that change the transcriptome and subsequent proliferative capacities of microglia. This observation opens up new opportunities for therapy aimed at disrupting this form of communication between tumor cells and surrounding cells, including tumor-associated microglia. It is proof that miRNAs can be transferred by EVs to cells in the brain *in vivo* with functional consequences.

STAR★METHODS

Detailed methods are provided in the online version of this paper and include the following:

- KEY RESOURCES TABLE
- LEAD CONTACT AND MATERIALS AVAILABILITY
- EXPERIMENTAL MODEL AND SUBJECT DETAILS
  - Animals
- CELL CULTURE
- PRIMARY MICROGLIA CULTURE
- METHOD DETAILS
  - Lentiviral Transduction Reporter
  - Proliferation assay
  - Vesicle Isolation Including Iodixanol Density Gradient
  - Intracranial Tumor Injection
  - Tissue Digestion
  - Flow Cytometry Preparation
  - Image Stream Analysis
  - Intracranial Injection of EVs
  - RT-qPCR
  - Digital Droplet PCR (ddPCR)
  - RNA Sequencing
- QUANTIFICATION AND STATISTICAL ANALYSIS
  - Data Processing and Analysis
- DATA AND CODE AVAILABILITY

SUPPLEMENTAL INFORMATION

Supplemental Information can be found online at https://doi.org/10.1016/j.celrep.2019.08.036.

ACKNOWLEDGMENTS

This publication is part of the NIH Extracellular RNA Communication Consortium paper package and was supported by the NIH Common Fund's exRNA Communication Program. We thank the Massachusetts General Hospital, Department of Pathology Flow and Image Cytometry Research Core, specifically Rachel Servis and Dr. Ravi Mylvaganam for their help and execution of the flow cytometry experiments. All members of the Breakefield laboratory who suggested ideas during laboratory meetings are very much appreciated. We also thank Dr. Thorsten Mempel for providing the H2B.mRFP plasmid. We thank Ms. Suzanne McDavitt for skilled editorial assistance. The Breakefield laboratory acknowledges grant support from NIH NCI CA179563, CA069246, and CA232103. The Krichevsky laboratory acknowledges grant support from NIH grants U19 CA179563, R01 CA215072, and R21 NS098051. Grant U19 CA179563 was supported by the NIH Common Fund, through the Office of Strategic Coordination/Office of the NIH Director. The MGH Vector Core was supported by NIH NINDS grant P30 NS045776.

The MGH Department of Pathology Flow and Image Cytometry Research Core obtained support from the NIH Shared Instrumentation Program with grants 1S10OD012027-01A1, 1S10OD016372-01, 1S10RR020936-01, and 1S10RR023440-01A1. Graphical illustrations in figures are derived from Servier Medical Art by Servier (https://smart.servier.com/) licensed under a Creative Commons Attribution 3.0 Unported License (https://creativecommons.org/licenses/by/3.0/).

AUTHOR CONTRIBUTIONS

E.R.A., S.L.N.M., X.O.B., M.L.D.B., and A.M.K. conceived the study. E.R.A., S.L.N.M., and X.O.B. designed the experiments. E.R.A., Z.W., L.N., P.S.C., and C.-J.K. performed and analyzed experiments. S.A.D. assisted during animal experiments. D.T.T. and E.T. assisted and performed RNA sequencing (RNA-seq) experiments. S.L.N.M. and E.T. performed the computational and statistical analysis of RNA-seq data. S.H. and J.E.K. provided advice on microglial isolation. X.O.B., M.L.D.B., and A.M.K. supervised the project. E.R.A. prepared figures. E.R.A. wrote the manuscript. All authors edited or commented on the manuscript.

DECLARATION OF INTERESTS

The authors declare no competing interests.

Received: March 11, 2019
Revised: July 9, 2019
Accepted: August 9, 2019
Published: September 17, 2019

SUPPORTING CITATIONS

The following references appear in the Supplemental Information: Afonso et al. (2018); Ahmed et al. (2011); Chen et al. (2016); Fiorentino et al. (2013); Hatley et al. (2010); He et al. (2016); Hu et al. (2008); Hu et al. (2017); Johnston et al. (2017); Kölling et al. (2017); Li et al. (2013); Liang et al. (2012); Liu et al. (2011); Lorenzen et al. (2015); Lu et al. (2008); Lu et al. (2009); Luo et al. (2014); Marquez et al. (2010); McDonald et al. (2013); Ng et al. (2012); Roy et al. (2009); Ruan et al. (2014); Sawant et al. (2013); Sayed et al. (2008); Sayed et al. (2010); Shi et al. (2013); Singh et al. (2015); Soares et al. (2014); Song et al. (2010); Sugatani et al. (2011); Thum et al. (2008); Wang et al. (2013); Wang et al. (2015); Wang et al. (2016); Wu et al. (2012); Wu et al. (2015); Xie et al. (2016); Yang et al. (2011); Yang et al. (2018); Ye et al. (2014).

REFERENCES

Abels, E.R., Broekman, M.L.D., Breakefield, X.O., and Maas, S.L.N. (2019). Glioma EVs contribute to immune privilege in the brain. Trends Cancer *5*, 393–396.

Afonso, M.B., Rodrigues, P.M., Simão, A.L., Gaspar, M.M., Carvalho, T., Borralho, P., Bañales, J.M., Castro, R.E., and Rodrigues, C.M.P. (2018). miRNA-21 ablation protects against liver injury and necroptosis in cholestasis. Cell Death Differ. *25*, 857–872.

Ahmed, M.I., Mardaryev, A.N., Lewis, C.J., Sharov, A.A., and Botchkareva, N.V. (2011). MicroRNA-21 is an important downstream component of BMP signalling in epidermal keratinocytes. J. Cell Sci. *124*, 3399–3404.

Akers, J.C., Gonda, D., Kim, R., Carter, B.S., and Chen, C.C. (2013). Biogenesis of extracellular vesicles (EV): exosomes, microvesicles, retrovirus-like vesicles, and apoptotic bodies. J. Neurooncol. *113*, 1–11.

Al-Nedawi, K., Meehan, B., Micallef, J., Lhotak, V., May, L., Guha, A., and Rak, J. (2008). Intercellular transfer of the oncogenic receptor EGFRvIII by microvesicles derived from tumour cells. Nat. Cell Biol. *10*, 619–624.

Belter, A., Rolle, K., Piwecka, M., Fedoruk-Wyszomirska, A., Naskręt-Barciszewska, M.Z., and Barciszewski, J. (2016). Inhibition of miR-21 in glioma cells using catalytic nucleic acids. Sci. Rep. *6*, 24516.

Bennett, M.L., Bennett, F.C., Liddelow, S.A., Ajami, B., Zamanian, J.L., Fernhoff, N.B., Mulinyawe, S.B., Bohlen, C.J., Adil, A., Tucker, A., et al. (2016). New tools for studying microglia in the mouse and human CNS. Proc. Natl. Acad. Sci. U S A *113*, E1738–E1746.

Bowman, R.L., Klemm, F., Akkari, L., Pyonteck, S.M., Sevenich, L., Quail, D.F., Dhara, S., Simpson, K., Gardner, E.E., Iacobuzio-Donahue, C.A., et al. (2016). Macrophage ontogeny underlies differences in tumor-specific education in brain malignancies. Cell Rep. *17*, 2445–2459.

Broekman, M.L., Maas, S.L.N., Abels, E.R., Mempel, T.R., Krichevsky, A.M., and Breakefield, X.O. (2018). Multidimensional communication in the microenvirons of glioblastoma. Nat. Rev. Neurol. *14*, 482–495.

Chan, J.A., Krichevsky, A.M., and Kosik, K.S. (2005). MicroRNA-21 is an antiapoptotic factor in human glioblastoma cells. Cancer Res. *65*, 6029–6033.

Chen, H., and Boutros, P.C. (2011). VennDiagram: a package for the generation of highly-customizable Venn and Euler diagrams in R. BMC Bioinformatics *12*, 35.

Chen, X., Song, M., Chen, W., Dimitrova-Shumkovska, J., Zhao, Y., Cao, Y., Song, Y., Yang, W., Wang, F., Xiang, Y., and Yang, C. (2016). MicroRNA-21 contributes to liver regeneration by targeting PTEN. Med. Sci. Monit. *22*, 83–91.

Chou, C.-H., Shrestha, S., Yang, C.-D., Chang, N.-W., Lin, Y.-L., Liao, K.-W., Huang, W.-C., Sun, T.-H., Tu, S.-J., Lee, W.-H., et al. (2018). miRTarBase update 2018: a resource for experimentally validated microRNA-target interactions. Nucleic Acids Res. *46* (*D1*), D296–D302.

Cocucci, E., and Meldolesi, J. (2015). Ectosomes and exosomes: shedding the confusion between extracellular vesicles. Trends Cell Biol. *25*, 364–372.

Conway, J.R., Lex, A., and Gehlenborg, N. (2017). UpSetR: an R package for the visualization of intersecting sets and their properties. Bioinformatics *33*, 2938–2940.

Corsten, M.F., Miranda, R., Kasmieh, R., Krichevsky, A.M., Weissleder, R., and Shah, K. (2007). MicroRNA-21 knockdown disrupts glioma growth in vivo and displays synergistic cytotoxicity with neural precursor cell delivered S-TRAIL in human gliomas. Cancer Res. *67*, 8994–9000.

de Vrij, J., Maas, S.L.N., Kwappenberg, K.M.C., Schnoor, R., Kleijn, A., Dekker, L., Luider, T.M., de Witte, L.D., Litjens, M., van Strien, M.E., et al. (2015). Glioblastoma-derived extracellular vesicles modify the phenotype of monocytic cells. Int. J. Cancer *137*, 1630–1642.

Dobin, A., Davis, C.A., Schlesinger, F., Drenkow, J., Zaleski, C., Jha, S., Batut, P., Chaisson, M., and Gingeras, T.R. (2013). STAR: ultrafast universal RNA-seq aligner. Bioinformatics *29*, 15–21.

Dweep, H., and Gretz, N. (2015). miRWalk2.0: a comprehensive atlas of microRNA-target interactions. Nat. Methods *12*, 697.

Dweep, H., Sticht, C., Pandey, P., and Gretz, N. (2011). miRWalk—database: prediction of possible miRNA binding sites by "walking" the genes of three genomes. J. Biomed. Inform. *44*, 839–847.

El Fatimy, R., Subramanian, S., Uhlmann, E.J., and Krichevsky, A.M. (2017). Genome editing reveals glioblastoma addiction to microRNA-10b. Mol. Ther. *25*, 368–378.

Farioli-Vecchioli, S., Tanori, M., Micheli, L., Mancuso, M., Leonardi, L., Saran, A., Ciotti, M.T., Ferretti, E., Gulino, A., Pazzaglia, S., and Tirone, F. (2007). Inhibition of medulloblastoma tumorigenesis by the antiproliferative and pro-differentiative gene PC3. FASEB J. *21*, 2215–2225.

Febinger, H.Y., Thomasy, H.E., Pavlova, M.N., Ringgold, K.M., Barf, P.R., George, A.M., Grillo, J.N., Bachstetter, A.D., Garcia, J.A., Cardona, A.E., et al. (2015). Time-dependent effects of CX3CR1 in a mouse model of mild traumatic brain injury. J. Neuroinflammation *12*, 154.

Fiorentino, L., Cavalera, M., Mavilio, M., Conserva, F., Menghini, R., Gesualdo, L., and Federici, M. (2013). Regulation of TIMP3 in diabetic nephropathy: a role for microRNAs. Acta Diabetol. *50*, 965–969.

Fitzner, D., Schnaars, M., van Rossum, D., Krishnamoorthy, G., Dibaj, P., Bakhti, M., Regen, T., Hanisch, U.-K., and Simons, M. (2011). Selective transfer of exosomes from oligodendrocytes to microglia by macropinocytosis. J. Cell Sci. *124*, 447–458.

Fujita, S., Ito, T., Mizutani, T., Minoguchi, S., Yamamichi, N., Sakurai, K., and Iba, H. (2008). miR-21 Gene expression triggered by AP-1 is sustained through a double-negative feedback mechanism. J. Mol. Biol. *378*, 492–504.

Gabriely, G., Wurdinger, T., Kesari, S., Esau, C.C., Burchard, J., Linsley, P.S., and Krichevsky, A.M. (2008). MicroRNA 21 promotes glioma invasion by targeting matrix metalloproteinase regulators. Mol. Cell. Biol. *28*, 5369–5380.

Gao, X., Li, X., Qian, C., Li, F., Zhang, Y., Dang, L., Xiao, X., Liu, F., Li, H., and Zhang, X. (2016). MiR-21 functions oppositely in proliferation and differentiation of neural stem/precursor cells via regulating AKT and GSK-3β. Cell. Mol. Biol. *62*, 144–149.

Guardavaccaro, D., Corrente, G., Covone, F., Micheli, L., D'Agnano, I., Starace, G., Caruso, M., and Tirone, F. (2000). Arrest of G(1)-S progression by the p53-inducible gene PC3 is Rb dependent and relies on the inhibition of cyclin D1 transcription. Mol. Cell. Biol. *20*, 1797–1815.

Hambardzumyan, D., Gutmann, D.H., and Kettenmann, H. (2016). The role of microglia and macrophages in glioma maintenance and progression. Nat. Neurosci. *19*, 20–27.

Hammond, T.R., Dufort, C., Dissing-Olesen, L., Giera, S., Young, A., Wysoker, A., Walker, A.J., Gergits, F., Segel, M., Nemesh, J., et al. (2019). Single-cell RNA sequencing of microglia throughout the mouse lifespan and in the injured brain reveals complex cell-state changes. Immunity *50*, 253–271.e6.

Hatley, M.E., Patrick, D.M., Garcia, M.R., Richardson, J.A., Bassel-Duby, R., van Rooij, E., and Olson, E.N. (2010). Modulation of K-Ras-dependent lung tumorigenesis by MicroRNA-21. Cancer Cell *18*, 282–293.

He, X., Zhang, K., Gao, X., Li, L., Tan, H., Chen, J., and Zhou, Y. (2016). Rapid atrial pacing induces myocardial fibrosis by down-regulating Smad7 via microRNA-21 in rabbit. Heart Vessels *31*, 1696–1708.

Hu, S.-J., Ren, G., Liu, J.-L., Zhao, Z.-A., Yu, Y.-S., Su, R.-W., Ma, X.-H., Ni, H., Lei, W., and Yang, Z.-M. (2008). MicroRNA expression and regulation in mouse uterus during embryo implantation. J. Biol. Chem. *283*, 23473–23484.

Hu, B., Wang, X., Hu, S., Ying, X., Wang, P., Zhang, X., Wang, J., Wang, H., and Wang, Y. (2017). miR-21-mediated radioresistance occurs via promoting repair of DNA double strand breaks. J. Biol. Chem. *292*, 3531–3540.

Johnston, D.G.W., Kearney, J., Zasłona, Z., Williams, M.A., O'Neill, L.A.J., and Corr, S.C. (2017). MicroRNA-21 limits uptake of *Listeria monocytogenes* by macrophages to reduce the intracellular niche and control infection. Front. Cell. Infect. Microbiol. *7*, 201.

Kölling, M., Kaucsar, T., Schauerte, C., Hübner, A., Dettling, A., Park, J.-K., Busch, M., Wulff, X., Meier, M., Scherf, K., et al. (2017). Therapeutic miR-21 silencing ameliorates diabetic kidney disease in mice. Mol. Ther. *25*, 165–180.

Kowal, J., Arras, G., Colombo, M., Jouve, M., Morath, J.P., Primdal-Bengtson, B., Dingli, F., Loew, D., Tkach, M., and Théry, C. (2016). Proteomic comparison defines novel markers to characterize heterogeneous populations of extracellular vesicle subtypes. Proc. Natl. Acad. Sci. U S A *113*, E968–E977.

Krichevsky, A.M., and Gabriely, G. (2009). miR-21: a small multi-faceted RNA. J. Cell. Mol. Med. *13*, 39–53.

Kumarswamy, R., Volkmann, I., and Thum, T. (2011). Regulation and function of miRNA-21 in health and disease. RNA Biol. *8*, 706–713.

Lai, C.P., Kim, E.Y., Badr, C.E., Weissleder, R., Mempel, T.R., Tannous, B.A., and Breakefield, X.O. (2015). Visualization and tracking of tumour extracellular vesicle delivery and RNA translation using multiplexed reporters. Nat. Commun. *6*, 7029.

Li, Q., and Barres, B.A. (2018). Microglia and macrophages in brain homeostasis and disease. Nat. Rev. Immunol. *18*, 225–242.

Li, W., and Graeber, M.B. (2012). The molecular profile of microglia under the influence of glioma. Neuro-oncol. *14*, 958–978.

Li, Q., Zhang, D., Wang, Y., Sun, P., Hou, X., Larner, J., Xiong, W., and Mi, J. (2013). MiR-21/Smad 7 signaling determines TGF-β1-induced CAF formation. Sci. Rep. *3*, 2038.

Liang, H., Zhang, C., Ban, T., Liu, Y., Mei, L., Piao, X., Zhao, D., Lu, Y., Chu, W., and Yang, B. (2012). A novel reciprocal loop between microRNA-21 and TGFβRIII is involved in cardiac fibrosis. Int. J. Biochem. Cell Biol. *44*, 2152–2160.

Liu, C., Li, B., Cheng, Y., Lin, J., Hao, J., Zhang, S., Mitchel, R.E.J., Sun, D., Ni, J., Zhao, L., et al. (2011). MiR-21 plays an important role in radiation induced carcinogenesis in BALB/c mice by directly targeting the tumor suppressor gene Big-h3. Int. J. Biol. Sci. *7*, 347–363.

Lorenzen, J.M., Schauerte, C., Hübner, A., Kölling, M., Martino, F., Scherf, K., Batkai, S., Zimmer, K., Foinquinos, A., Kaucsar, T., et al. (2015). Osteopontin is indispensible for AP1-mediated angiotensin II-related miR-21 transcription during cardiac fibrosis. Eur. Heart J. *36*, 2184–2196.

Love, M.I., Huber, W., and Anders, S. (2014). Moderated estimation of fold change and dispersion for RNA-seq data with DESeq2. Genome Biol. *15*, 550.

Lu, Z., Liu, M., Stribinskis, V., Klinge, C.M., Ramos, K.S., Colburn, N.H., and Li, Y. (2008). MicroRNA-21 promotes cell transformation by targeting the programmed cell death 4 gene. Oncogene *27*, 4373–4379.

Lu, T.X., Munitz, A., and Rothenberg, M.E. (2009). MicroRNA-21 is up-regulated in allergic airway inflammation and regulates IL-12p35 expression. J. Immunol. *182*, 4994–5002.

Luo, X., Gu, J., Zhu, R., Feng, M., Zhu, X., Li, Y., and Fei, J. (2014). Integrative analysis of differential miRNA and functional study of miR-21 by seed-targeting inhibition in multiple myeloma cells in response to berberine. BMC Syst. Biol. *8*, 82.

Ma, X., Kumar, M., Choudhury, S.N., Becker Buscaglia, L.E., Barker, J.R., Kanakamedala, K., Liu, M.-F., and Li, Y. (2011). Loss of the miR-21 allele elevates the expression of its target genes and reduces tumorigenesis. Proc. Natl. Acad. Sci. U S A *108*, 10144–10149.

Maas, S.L.N., Breakefield, X.O., and Weaver, A.M. (2017). Extracellular vesicles: unique intercellular delivery vehicles. Trends Cell Biol. *27*, 172–188.

Marquez, R.T., Wendlandt, E., Galle, C.S., Keck, K., and McCaffrey, A.P. (2010). MicroRNA-21 is upregulated during the proliferative phase of liver regeneration, targets Pellino-1, and inhibits NF-kappaB signaling. Am. J. Physiol. Gastrointest. Liver Physiol. *298*, G535–G541.

Mateescu, B., Kowal, E.J.K., van Balkom, B.W.M., Bartel, S., Bhattacharyya, S.N., Buzás, E.I., Buck, A.H., de Candia, P., Chow, F.W.N., Das, S., et al. (2017). Obstacles and opportunities in the functional analysis of extracellular vesicle RNA - an ISEV position paper. J. Extracell. Vesicles *6*, 1286095.

Matsuda, S., Rouault, J., Magaud, J., and Berthet, C. (2001). In search of a function for the TIS21/PC3/BTG1/TOB family. FEBS Lett. *497*, 67–72.

McCabe, J.B., and Berthiaume, L.G. (1999). Functional roles for fatty acylated amino-terminal domains in subcellular localization. Mol. Biol. Cell *10*, 3771–3786.

McDonald, R.A., White, K.M., Wu, J., Cooley, B.C., Robertson, K.E., Halliday, C.A., McClure, J.D., Francis, S., Lu, R., Kennedy, S., et al. (2013). miRNA-21 is dysregulated in response to vein grafting in multiple models and genetic ablation in mice attenuates neointima formation. Eur. Heart J. *34*, 1636–1643.

McNamara, R.P., Costantini, L.M., Myers, T.A., Schouest, B., Maness, N.J., Griffith, J.D., Damania, B.A., MacLean, A.G., and Dittmer, D.P. (2018). Nef Secretion into Extracellular Vesicles or Exosomes Is Conserved across Human and Simian Immunodeficiency Viruses. MBio *9*, 559.

Morantz, R.A., Wood, G.W., Foster, M., Clark, M., and Gollahon, K. (1979a). Macrophages in experimental and human brain tumors. Part 1: Studies of the macrophage content of experimental rat brain tumors of varying immunogenicity. J. Neurosurg. *50*, 298–304.

Morantz, R.A., Wood, G.W., Foster, M., Clark, M., and Gollahon, K. (1979b). Macrophages in experimental and human brain tumors. Part 2: studies of the macrophage content of human brain tumors. J. Neurosurg. *50*, 305–311.

Morton, M.C., Neckles, V.N., Seluzicki, C.M., Holmberg, J.C., and Feliciano, D.M. (2018). Neonatal subventricular zone neural stem cells release extracellular vesicles that act as a microglial morphogen. Cell Rep. *23*, 78–89.

Ng, R., Song, G., Roll, G.R., Frandsen, N.M., and Willenbring, H. (2012). A microRNA-21 surge facilitates rapid cyclin D1 translation and cell cycle progression in mouse liver regeneration. J. Clin. Invest. *122*, 1097–1108.

Nolte-'t Hoen, E.N.M., Buermans, H.P.J., Waasdorp, M., Stoorvogel, W., Wauben, M.H.M., and 't Hoen, P.A.C. (2012). Deep sequencing of RNA from immune cell-derived vesicles uncovers the selective incorporation of small

non-coding RNA biotypes with potential regulatory functions. Nucleic Acids Res. *40*, 9272–9285.

Ostrom, Q.T., Gittleman, H., Farah, P., Ondracek, A., Chen, Y., Wolinsky, Y., Stroup, N.E., Kruchko, C., and Barnholtz-Sloan, J.S. (2013). CBTRUS statistical report: Primary brain and central nervous system tumors diagnosed in the United States in 2006-2010. Neuro-oncol. *15* (*Suppl 2*), ii1–ii56.

Ostrom, Q.T., Gittleman, H., Truitt, G., Boscia, A., Kruchko, C., and Barnholtz-Sloan, J.S. (2018). CBTRUS statistical report: primary brain and other central nervous system tumors diagnosed in the United States in 2011-2015. Neuro-oncol. *20* (*suppl_4*), iv1–iv86.

Pepe, G., De Maglie, M., Minoli, L., Villa, A., Maggi, A., and Vegeto, E. (2017). Selective proliferative response of microglia to alternative polarization signals. J. Neuroinflammation *14*, 236.

Põlajeva, J., Swartling, F.J., Jiang, Y., Singh, U., Pietras, K., Uhrbom, L., Westermark, B., and Roswall, P. (2012). miRNA-21 is developmentally regulated in mouse brain and is co-expressed with SOX2 in glioma. BMC Cancer *12*, 378.

Quail, D.F., and Joyce, J.A. (2017). The microenvironmental landscape of brain tumors. Cancer Cell *31*, 326–341.

Roy, S., Khanna, S., Hussain, S.-R.A., Biswas, S., Azad, A., Rink, C., Gnyawali, S., Shilo, S., Nuovo, G.J., and Sen, C.K. (2009). MicroRNA expression in response to murine myocardial infarction: miR-21 regulates fibroblast metalloprotease-2 via phosphatase and tensin homologue. Cardiovasc. Res. *82*, 21–29.

Ruan, Q., Wang, P., Wang, T., Qi, J., Wei, M., Wang, S., Fan, T., Johnson, D., Wan, X., Shi, W., et al. (2014). MicroRNA-21 regulates T-cell apoptosis by directly targeting the tumor suppressor gene Tipe2. Cell Death Dis. *5*, e1095.

Sawant, D.V., Wu, H., Kaplan, M.H., and Dent, A.L. (2013). The Bcl6 target gene microRNA-21 promotes Th2 differentiation by a T cell intrinsic pathway. Mol. Immunol. *54*, 435–442.

Sayed, D., Rane, S., Lypowy, J., He, M., Chen, I.-Y., Vashistha, H., Yan, L., Malhotra, A., Vatner, D., and Abdellatif, M. (2008). MicroRNA-21 targets Sprouty2 and promotes cellular outgrowths. Mol. Biol. Cell *19*, 3272–3282.

Sayed, D., He, M., Hong, C., Gao, S., Rane, S., Yang, Z., and Abdellatif, M. (2010). MicroRNA-21 is a downstream effector of AKT that mediates its antiapoptotic effects via suppression of Fas ligand. J. Biol. Chem. *285*, 20281–20290.

Sena-Esteves, M., Tebbets, J.C., Steffens, S., Crombleholme, T., and Flake, A.W. (2004). Optimized large-scale production of high titer lentivirus vector pseudotypes. J. Virol. Methods *122*, 131–139.

Shi, C., Liang, Y., Yang, J., Xia, Y., Chen, H., Han, H., Yang, Y., Wu, W., Gao, R., and Qin, H. (2013). MicroRNA-21 knockout improve the survival rate in DSS induced fatal colitis through protecting against inflammation and tissue injury. PLoS ONE *8*, e66814.

Shi, R., Wang, P.-Y., Li, X.-Y., Chen, J.-X., Li, Y., Zhang, X.-Z., Zhang, C.-G., Jiang, T., Li, W.-B., Ding, W., and Cheng, S.J. (2015). Exosomal levels of miRNA-21 from cerebrospinal fluids associated with poor prognosis and tumor recurrence of glioma patients. Oncotarget *6*, 26971–26981.

Singh, S.K., Marisetty, A., Sathyan, P., Kagalwala, M., Zhao, Z., and Majumder, S. (2015). REST-miR-21-SOX2 axis maintains pluripotency in E14Tg2a.4 embryonic stem cells. Stem Cell Res. (Amst.) *15*, 305–311.

Skog, J., Würdinger, T., van Rijn, S., Meijer, D.H., Gainche, L., Sena-Esteves, M., Curry, W.T., Jr., Carter, B.S., Krichevsky, A.M., and Breakefield, X.O. (2008). Glioblastoma microvesicles transport RNA and proteins that promote tumour growth and provide diagnostic biomarkers. Nat. Cell Biol. *10*, 1470–1476.

Soares, R.J., Cagnin, S., Chemello, F., Silvestrin, M., Musaro, A., De Pitta, C., Lanfranchi, G., and Sandri, M. (2014). Involvement of microRNAs in the regulation of muscle wasting during catabolic conditions. J. Biol. Chem. *289*, 21909–21925.

Song, G., Sharma, A.D., Roll, G.R., Ng, R., Lee, A.Y., Blelloch, R.H., Frandsen, N.M., and Willenbring, H. (2010). MicroRNAs control hepatocyte proliferation during liver regeneration. Hepatology *51*, 1735–1743.

Stupp, R., Hegi, M.E., Mason, W.P., van den Bent, M.J., Taphoorn, M.J.B., Janzer, R.C., Ludwin, S.K., Allgeier, A., Fisher, B., Belanger, K., et al.; European Organisation for Research and Treatment of Cancer Brain Tumour and Radiation Oncology Groups; National Cancer Institute of Canada Clinical Trials Group (2009). Effects of radiotherapy with concomitant and adjuvant temozolomide versus radiotherapy alone on survival in glioblastoma in a randomised phase III study: 5-year analysis of the EORTC-NCIC trial. Lancet Oncol. *10*, 459–466.

Sugatani, T., Vacher, J., and Hruska, K.A. (2011). A microRNA expression signature of osteoclastogenesis. Blood *117*, 3648–3657.

Tamashiro, T.T., Dalgard, C.L., and Byrnes, K.R. (2012). Primary microglia isolation from mixed glial cell cultures of neonatal rat brain tissue. J. Vis. Exp. (*66*), e3814.

Teplyuk, N.M., Mollenhauer, B., Gabriely, G., Giese, A., Kim, E., Smolsky, M., Kim, R.Y., Saria, M.G., Pastorino, S., Kesari, S., and Krichevsky, A.M. (2012). MicroRNAs in cerebrospinal fluid identify glioblastoma and metastatic brain cancers and reflect disease activity. Neuro-oncol. *14*, 689–700.

Théry, C., Witwer, K.W., Aikawa, E., Alcaraz, M.J., Anderson, J.D., Andriantsitohaina, R., Antoniou, A., Arab, T., Archer, F., Atkin-Smith, G.K., et al. (2018). Minimal information for studies of extracellular vesicles 2018 (MISEV2018): a position statement of the International Society for Extracellular Vesicles and update of the MISEV2014 guidelines. J. Extracell. Vesicles *7*, 1535750.

Thum, T., Gross, C., Fiedler, J., Fischer, T., Kissler, S., Bussen, M., Galuppo, P., Just, S., Rottbauer, W., Frantz, S., et al. (2008). MicroRNA-21 contributes to myocardial disease by stimulating MAP kinase signalling in fibroblasts. Nature *456*, 980–984.

Tkach, M., and Théry, C. (2016). Communication by extracellular vesicles: where we are and where we need to go. Cell *164*, 1226–1232.

Valadi, H., Ekström, K., Bossios, A., Sjöstrand, M., Lee, J.J., and Lötvall, J.O. (2007). Exosome-mediated transfer of mRNAs and microRNAs is a novel mechanism of genetic exchange between cells. Nat. Cell Biol. *9*, 654–659.

van der Vos, K.E., Abels, E.R., Zhang, X., Lai, C., Carrizosa, E., Oakley, D., Prabhakar, S., Mardini, O., Crommentuijn, M.H.W., Skog, J., et al. (2016). Directly visualized glioblastoma-derived extracellular vesicles transfer RNA to microglia/macrophages in the brain. Neuro-oncol. *18*, 58–69.

Vickers, K.C., Palmisano, B.T., Shoucri, B.M., Shamburek, R.D., and Remaley, A.T. (2011). MicroRNAs are transported in plasma and delivered to recipient cells by high-density lipoproteins. Nat. Cell Biol. *13*, 423–433.

Wang, J., Gao, Y., Ma, M., Li, M., Zou, D., Yang, J., Zhu, Z., and Zhao, X. (2013). Effect of miR-21 on renal fibrosis by regulating MMP-9 and TIMP1 in kk-ay diabetic nephropathy mice. Cell Biochem. Biophys. *67*, 537–546.

Wang, Z., Brandt, S., Medeiros, A., Wang, S., Wu, H., Dent, A., and Serezani, C.H. (2015). MicroRNA 21 is a homeostatic regulator of macrophage polarization and prevents prostaglandin E2-mediated M2 generation. PLoS ONE *10*, e0115855.

Wang, P., Zhao, Y., Fan, R., Chen, T., and Dong, C. (2016). MicroRNA-21a-5p functions on the regulation of melanogenesis by targeting Sox5 in mouse skin melanocytes. Int. J. Mol. Sci. *17*, 959.

Wei, F., Yang, S., Guo, Q., Zhang, X., Ren, D., Lv, T., and Xu, X. (2017a). MicroRNA-21 regulates Osteogenic Differentiation of Periodontal Ligament Stem Cells by targeting Smad5. Sci. Rep. *7*, 16608.

Wei, Z., Batagov, A.O., Schinelli, S., Wang, J., Wang, Y., El Fatimy, R., Rabinovsky, R., Balaj, L., Chen, C.C., Hochberg, F., et al. (2017b). Coding and noncoding landscape of extracellular RNA released by human glioma stem cells. Nat. Commun. *8*, 1145.

Weller, M., Wick, W., Aldape, K., Brada, M., Berger, M., Pfister, S.M., Nishikawa, R., Rosenthal, M., Wen, P.Y., Stupp, R., and Reifenberger, G. (2015). Glioma. Nat. Rev. Dis. Primers *1*, 15017.

Welm, B.E., Dijkgraaf, G.J.P., Bledau, A.S., Welm, A.L., and Werb, Z. (2008). Lentiviral transduction of mammary stem cells for analysis of gene function during development and cancer. Cell Stem Cell *2*, 90–102.

Winter, J., Jung, S., Keller, S., Gregory, R.I., and Diederichs, S. (2009). Many roads to maturity: microRNA biogenesis pathways and their regulation. Nat. Cell Biol. *11*, 228–234.

Wu, Z., Lu, H., Sheng, J., and Li, L. (2012). Inductive microRNA-21 impairs anti-mycobacterial responses by targeting IL-12 and Bcl-2. FEBS Lett. *586*, 2459–2467.

Wu, T., Liu, Y., Fan, Z., Xu, J., Jin, L., Gao, Z., Wu, Z., Hu, L., Wang, J., Zhang, C., et al. (2015). miR-21 modulates the immunoregulatory function of bone marrow mesenchymal stem cells through the PTEN/Akt/TGF-β1 pathway. Stem Cells *33*, 3281–3290.

Xie, X., Song, J., and Li, G. (2016). MiR-21a-5p suppresses bisphenol A-induced pre-adipocyte differentiation by targeting map2k3 through MKK3/p38/MAPK. Biochem. Biophys. Res. Commun. *473*, 140–146.

Yang, C.H., Yue, J., Pfeffer, S.R., Handorf, C.R., and Pfeffer, L.M. (2011). MicroRNA miR-21 regulates the metastatic behavior of B16 melanoma cells. J. Biol. Chem. *286*, 39172–39178.

Yang, C.H., Yue, J., Pfeffer, S.R., Fan, M., Paulus, E., Hosni-Ahmed, A., Sims, M., Qayyum, S., Davidoff, A.M., Handorf, C.R., and Pfeffer, L.M. (2014). MicroRNA-21 promotes glioblastoma tumorigenesis by down-regulating insulin-like growth factor-binding protein-3 (IGFBP3). J. Biol. Chem. *289*, 25079–25087.

Yang, L., Wang, B., Zhou, Q., Wang, Y., Liu, X., Liu, Z., and Zhan, Z. (2018). MicroRNA-21 prevents excessive inflammation and cardiac dysfunction after myocardial infarction through targeting KBTBD7. Cell Death Dis. *9*, 769.

Ye, X., Zhang, H.M., Qiu, Y., Hanson, P.J., Hemida, M.G., Wei, W., Hoodless, P.A., Chu, F., and Yang, D. (2014). Coxsackievirus-induced miR-21 disrupts cardiomyocyte interactions via the downregulation of intercalated disk components. PLoS Pathog. *10*, e1004070.

STAR★METHODS

KEY RESOURCES TABLE

REAGENT or RESOURCE	SOURCE	IDENTIFIER
Antibodies		
Rabbit monoclonal TSG101	Abcam	Cat# ab125011 RRID:AB_10974262
Mouse monoclonal ALIX	Santa Cruz	Cat# sc53538 RRID:AB_673821
Rabbit monoclonal FLOTILLIN-1	Abcam	Cat# ab133497 RRID:AB_11156367
Mouse monoclonal GAPDH	Millipore Sigma	Cat#: CB1001 RRID:AB_2107426
Rabbit polyclonal GFP Tag	Thermo Fisher	Cat# A-11122; RRID:AB _221569
Rabbit polyclonal Ki67	Abcam	Cat# ab15580; RRID:AB_443209
ECL Anti-rabbit IgG	Sigma	Cat# GENA934-1ML RRID:AB_2722659
ECL Anti-mouse IgG	Thermo Fisher	Cat# GENA931-1ML
goat-anti-rat Alexa Fluor 647	Abcam	Cat# ab150155
anti-CD45-PE-Cy7	BioLegend	Cat# 103113, clone 30-F11 RRID:AB_312978
anti-CD45-PE	BioLegend	Cat# 103105, clone 30-F11 RRID:AB_312970
anti-CD11b- Alexa Fluor 647	BioLegend	Cat# 101220, clone M1/70; RRID:AB_493546
anti-CD11b-PE	BioLegend	Cat# 101207, clone M1/70; RRID:AB_312790
anti-CD11b-PE-Cy7	BioLegend	Cat# 101215, clone M1/70; RRID:AB_312798
anti-GFP-Alexa Fluor 647	BioLegend	Cat# 338005, clone FM264G RRID:AB_1279413
anti-GFAP-Alexa Fluor 488	Thermo Fisher	Cat# 53-9892-80, clone GA5 RRID:AB_10597754
TruStain fcX	BioLegend	Cat# 101320, clone 93; RRID:AB_1574975
Virus Strains		
VSV-G Pseudotyped Lentivirus	Sena-Esteves et al., 2004	Breakefield lab
Chemicals, Peptides, and Recombinant Proteins		
Dulbecco's modified Eagle's medium (DMEM)	Corning	Cat# 10-013-CV
Roswell Park Memorial Institute (RPMI) 1640 with L-glutamine (no phenol red)	Fisher Scientific	Cat# 11835030
Fetal bovine serum (FBS)	Gemini Bioproducts	Cat# 900-208 Lot# A78E00G
Penicillin (100 units/ml) and Streptomycin (100 μg/ml) (P/S)	Corning	Cat# 30-002-CI
OptiMEM	GIBCO	Cat# 31985-062
0.05% Trypsin/0.53mM EDTA in HBSS w/o calcium, magnesium or sodium bicarbonate	Corning	Cat# MT25052CI
Trypsin-EDTA (0.25%), phenol red	Fisher Scientific	Cat# 25200056
DharmaFECT 1 Transfection Reagent	Dharmacon	Cat# T-2001-01
M-CSF recombinant mouse protein	Thermo Fisher	Cat. # PMC2044
cOmplete, Mini, EDTA-free protease inhibitor cocktail	Sigma-Aldrich	Cat# 4693159001
Phosphate buffered saline (PBS) 10X	Boston Bioproducts	Cat# BM-220
Ketamine	Bioniche Pharma	Cat# NPC 67457-001-10
Xylazine	Santa Cruz	Cat# sc-362950Rx
PFA 32%	Electron Microscopy Sciences	Cat# 100496-496
poly-D-lysine	Sigma-Aldrich	Cat# P7405-5MG
ProLong® diamond antifade mountant	Thermo Fisher	Cat# P36965
DAPI	Thermo Fisher	Cat# D1306
RBC lysis buffer	Boston BioProducts	Cat# IBB-198
DPBS without Mg^{2+} and Ca^{2+}	Corning	Cat# 21-031-CV

(*Continued on next page*)

Continued

REAGENT or RESOURCE	SOURCE	IDENTIFIER
2-mercaptoethanol	Sigma Aldrich	Cat# 133051
ERCC RNA Spike-In Mix	Life Technologies	Cat# 4456740
Agencourt AMPure XP beads	Beckman Coulter	Cat# A63880
OptiPrep Density Gradient Medium	Sigma Aldrich	Cat# D1556
VECTASHIELD® Antifade Mounting Medium	Vector Labs	Cat# H-1000
Critical Commercial Assays		
RNeasy Plus Micro Kit (50)	QIAGEN	Cat# 74034
SMARTer Ultra Low Input RNA Kit for Sequencing – v3	Clontech	Cat# 634848, 634849, 634850, 634851, 634852 & 634853
Nextera® XT DNA Library Preparation kit	Illumina	Cat# FC-131-1096
SYBR® FAST Universal qPCR Kit	KAPA Biosystems	Cat# KK4600
NextSeq 500/550 High Output v2 kit	Illumina	Cat# FC-404-2002
1% PhiX Sequencing Control V3	Illumina	Cat# FC-110-3001
Neural Tissue Dissociation Kit (P)	Miltenyi Biotec	Cat# 130-092-628
BD Cytofix/Cytoperm	BD Biosciences	Cat# 554714
SuperScript VILO cDNA Synthesis Kit	Invitrogen	Cat# 11754050
Pierce BCA Protein Assay Kit	Thermo Fisher	Cat# 23225
SuperSignal West Pico PLUS Chemiluminescent Substrate	Thermo Fisher	Cat# 34580
ddPCR Supermix for Probes (No dUTP)	Bio-Rad	Cat# 1863024
Droplet Generation Oil for Probes	Bio-Rad	Cat# 1863005
DG8 Gaskets for QX200/QX100 Droplet Generator	Bio-Rad	Cat# 1863009
DG8 Cartridges for QX200/QX100 Droplet Generator	Bio-Rad	Cat# 1864008
Deposited Data		
RNA seq raw data (FastQ files)	This paper	GSE12607
RNA seq processed data	This paper	GSE12607
R script git repository	This paper	https://github.com/slnmaas/miR21-Project
Experimental Models: Cell Lines		
GL261	NCI Tumor Repository	https://dtp.cancer.gov/repositories/
Experimental Models: Organisms/Strains		
B6;129S6-MiR-21atm1Yoli/J (miR-21-null)	The Jackson Laboratory	Kind gift from Dr. Anna Krichevsky
Oligonucleotides		
Oligonucleotides for qRT-PCR	This paper	Table S2
PrimePCR ddPCR Expression Probe Assay: Actb, Mouse	Bio-Rad	Unique Assay ID: dMmuCPE5195285
PrimePCR ddPCR Expression Probe Assay: Pdcd4, Mouse	Bio-Rad	Unique Assay ID: dMmuCPE5113532
PrimePCR ddPCR Expression Probe Assay: Btg2, Mouse	Bio-Rad	Unique Assay ID: qMmuCIP0029872
SMARTpool: ON-TARGETplus Btg2 siRNA	Dharmacon	Cat# L-043138-01-0005
ON-TARGETplus Non-targeting Pool	Dharmacon	Cat# D-001810-10-05
miRIDIAN microRNA mmu-miR-21a-5p mimic	Dharmacon	Cat# C-310515-05-0005
miRIDIAN microRNA Mimic Negative Control #1	Dharmacon	Cat# CN-001000-01-05
Recombinant DNA		
CSCW2.palmGFP	Lai et al., 2015; McCabe and Berthiaume, 1999	Breakefield lab
pHIV-H2BmRFP	Welm et al., 2008	Kind gift of Dr. Thorsten Mempel

(*Continued on next page*)

Continued

REAGENT or RESOURCE	SOURCE	IDENTIFIER
Software and Algorithms		
Zen Pro 2012	ZEISS	https://www.zeiss.com/microscopy/us/products/microscope-software/zen.html
ImageJ 1.49v	NIH	https://imagej-nih-gov.ezp-prod1.hul.harvard.edu/ij/
STAR v2.4.0h	Dobin et al., 2013	https://github.com/alexdobin/STAR
MarkDuplicates tool in picard-tools-1.8.4	Broad Institute	http://broadinstitute.github.io/picard/
Gencode GRCm38.p3 GTF annotations	Trust Sanger Institute	https://www.gencodegenes.org/mouse_releases/3.html
R (version 3.2.3)	The R Foundation	https://www.r-project.org/
R Studio	The R Foundation	https://www.rstudio.com/
DESeq2 (version 1.10)	Love et al., 2014	https://bioconductor.org/packages/release/bioc/html/DESeq2.html
gplots (version 2.17) heatmap.2 function		https://cran.r-project.org/web/packages/gplots/index.html
UpSetR (version 1.3.3)	Conway et al., 2017	https://cran.r-project.org/web/packages/UpSetR/index.html
VennDiagram (version 1.6.16)	Chen and Boutros, 2011	https://cran.r-project.org/web/packages/VennDiagram/index.html
Prism	GraphPad	https://www.graphpad.com/scientific-software/prism/
FlowJo	FlowJo	https://www.flowjo.com/
Other		
100 μm cell strainer	Thermo Fisher	Cat# 22363549
70 μm cell strainer	Corning	Cat# CLS431751
40 μm cell strainer	Corning	Cat# 352340
Quick-Seal® Polypropylene Tubes	Beckman Coulter	Cat# 342414
Thinwall Polypropylene Tubes	Beckman Coulter	Cat# 326819
Type 70 Ti Rotor	Beckman Coulter	Cat# 337922
MLS-50 Swinging-Bucket Rotor	Beckman Coulter	Cat# 367280
Optima Max-XP Ultracentrifuge	Beckman Coulter	Cat# 393315
Optima XE Ultracentrifuge	Beckman Coulter	Cat# A94471
GentleMacs C-tube	Miltenyi Biotec	Cat# 130-093-237
LS Columns	Miltenyi Biotec	Cat# 130-042-401
MidiMACS	Miltenyi Biotec	Cat# 130-042-301
gentleMACS Dissociator	Miltenyi Biotec	Cat# # 130-093-235
BD Falcon Tube with Cell Strainer Cap	BD Falcon	Cat# 08-771-23
BD FACSAria II SORP Cell Sorter	BD Falcon	N/A
QuantStudio 3 PCR system	Applied Biosciences	N/A
Agilent 2100 Bioanalyzer	Agilent Technologies	N/A
Amnis ImageStream mkII Imaging Flow Cytometer	EMD Millipore	N/A
NextSeq 500 sequencer	Illumina	N/A
Mycoplasma PCR Detection Kit	ABM	Cat# G238

LEAD CONTACT AND MATERIALS AVAILABILITY

This study did not generate new unique reagents. Further information and requests for resources and reagents should be directed to and will be fulfilled by the Lead Contact, Dr. Xandra O. Breakefield (breakefield@hms.harvard.edu).

EXPERIMENTAL MODEL AND SUBJECT DETAILS

Animals

All animal experiments were conducted under the oversight of the Massachusetts General Hospital Institution Animal Care and Use Committee. B6;129S6-MiR-21atm1Yoli/J (miR-21 null) mice were maintained with unlimited access to water and food under a 12-hour light/dark cycle (Ma et al., 2011). Male and female mice ranging from 12 - 14 weeks in age were randomly assigned to experimental groups. For RNA sequencing 3 mice were assigned per group. Injection of EVs was also done with 3 animals per group.

CELL CULTURE

Mouse glioma cell-line GL261 (NCI Tumor Repository) was cultured at 37°C in a 5% CO_2 humidified incubator. Culture media was comprised of Roswell Park Memorial Institute (RPMI) 1640 with L-glutamine (Corning) supplemented with penicillin (100 units/ml), streptomycin (100 μg/ml) (P/S) (Corning) and 10% fetal bovine serum (FBS) (Gemini Bioproducts). Cells were tested for mycoplasma contamination (Mycoplasma PCR Detection Kit, abm G238) and found negative. Cells grown for EV isolation were cultured in media supplemented with 5% EV-depleted FBS. FBS was depleted from EVs by 16 hours of ultracentrifugation at 160,000xg.

PRIMARY MICROGLIA CULTURE

Mixed glial cultures were isolated from cerebral cortices of P1 to P4 mouse pups. Meninges were removed, and cortical cells were dissociated using 0.05% Trypsin/EDTA (Corning) followed by cell straining using 100 μm and 40 μm cell strainers. Cells were cultured in DMEM with 20% FBS, 1% P/S and 10 ng/ml M-CSF (GIBCO) in poly-D-lysine (PDL; Sigma-Aldrich; 10 μg/ml) on pre-coated T-75 culture flasks for 10-15 days. Primary microglia were harvested from confluent mixed glial culture by gentle shaking on an orbital shaker for 30-60 min at 180 rpm and cultured in the same medium (Tamashiro et al., 2012).

METHOD DETAILS

Lentiviral Transduction Reporter

GL261 cells were stably transduced using a CSCW2 lentiviral vector (Sena-Esteves et al., 2004) encoding palmitoylated GFP (palmGFP), resulting in membrane localized GFP expression in cells and EVs released by these cells (Lai et al., 2015; McCabe and Berthiaume, 1999). A second transduction was performed to stably express the H2B.mRFP reporter (Addgene #18982, acquired from Dr. Thorsten Mempel, MGH) (Welm et al., 2008). Following transduction, cells were sorted for single cell cloning on the expression of both GFP and RFP. A clone with stable expression of both reporters was used for all experiments. For imaging of the cells, they were seeded on PDL (Sigma-Aldrich) coated glass coverslips and incubated for 48 hours. Cells were then washed in PBS and fixed using 4% paraformaldehyde (PFA; Electron Microscopy Sciences) in PBS. DAPI (1 μg/ml) (Thermo Fisher) staining was performed for 30 min at room temperature. Slides were washed for 10 min using PBS and mounted on microscopy slides using ProLong® Diamond Antifade Mountant (Thermo Fisher). Fluorescence microscopy images were acquired on the Zeiss Axio Imager M2 (Carl Zeiss).

Proliferation assay

miR-21 null primary microglia were seeded at the density of 70,000 cells/well on coverslips coated with poly-D-lysine (PDL; Sigma-Aldrich; 10 μg/ml). Microglia were transfected using DharmaFECT (Dharmacon) transfection reagent in Opti-MEM (GIBCO). miR-21 mimic and scrambled control were used at a concentration of 20 μM, siRNA against *Btg2* and siRNA control at 5 μM. Transfection mixes were incubated for 30 min before adding to the cells, which were subsequently incubated for 24 hours at 37°C. After incubation, microglia were washed in PBS for 5 min and fixed in 100% ice-cold methanol for 10 min. After fixation cells were washed two times in PBS for 5 min. Microglia were blocked in 5% BSA and 0.1% Triton X-100 (USB) in PBS (PBS-T) for 4 hours. Microglia were then incubated with the primary antibody Ki67 anti-rabbit (Abcam, 1:4000) at 4°C overnight. Microglia were washed three times in PBS-T for 5 min. Secondary antibody goat anti-rabbit (Invitrogen, 1:400) was diluted in PBS-T and incubated for 1 hour in dark at RT. Microglia were stained for DAPI (Thermo Fisher, 1 μg/ml) diluted in PBST and incubated for 5 min. Coverslips were transferred to microscope slides (Fisherbrand) on a droplet of mounting medium (Vectashield, Vector Labs). Fluorescence microscopy images were acquired on the Zeiss Axio Imager M2 (Carl Zeiss). Quantification of proliferation 24 hours was measured as Ki67 positive cells per total number of DAPI positive cells using ImageJ.

Vesicle Isolation Including Iodixanol Density Gradient

The differential ultracentrifugation protocol consisted of subsequent centrifugation at 300xg for 10 min and 2000xg 10 min. Two-thousand xg pellet was collected and resuspended in PBS or RIPA buffer respectively for injection or western blot analysis. Supernatants were filtered through 0.8μm filter (Sigma) and centrifuged for 100,000xg (*k*-factor of 220.1) 120 min in Quick-Seal® Polypropylene Tubes (Beckman) using Type 70 Ti in Optima XE ultracentrifuge (Beckman) to pellet EVs. For EV exposure experiments and

western blot analysis, pellets were resuspended in remaining supernatant supplemented with OptiMEM and concentrated by centrifugation at 100,000xg (*k*-factor of 190.7) for 120 min in Thinwall Polypropylene Tubes (Beckman) using MLS-50 Swinging-Bucket Rotor (Beckman) in an Optima Max-XP Ultracentrifuge. Final EV pellet was resuspended in DPBS for exposure experiment or RIPA buffer for western blot analysis.

Prior to western blot analysis cells and EVs were lysed in RIPA buffer with protease inhibitors (Sigma). Protein concentration was determined using Pierce BCA protein assay (Thermo Fisher) and equal amounts were loaded and resolved on 10% SDS-PAGE gel (Thermo Fisher). After transfer onto nitrocellulose membranes, samples were probed for GFP (Thermo Fisher, A-11120, 1:1000), GAPDH (Millipore, CB1001, 1:1000), TSG101 (Abcam, ab125011, 1:500), ALIX (Santa Cruz, sc-53538, 1:200) and Flotillin-1 (Abcam, ab133497, 1:500). ECL Anti-Rabbit IgG (Sigma) and ECL Anti-mouse IgG (Thermo Fisher) corresponding to the primary antibody were used as a secondary antibody.

For iodixanol density gradient the 100,000xg EV pellet was resuspended in 300 μl supernatant and mixed by adding 1 mL 60% cold iodixanol (OptiPrep Density Gradient Medium, Sigma D1556), the mixture was subsequently transferred to a Thinwall Polypropylene Tubes (Beckman). One layer of 500 μl of 40% and 30% iodixanol (diluted with 10x PBS and Milli-Q) were loaded on top of the 46% layer consisting EVs in the suspension of 60% iodixanol. The remaining volume was filled using 10% iodixanol. The density step-gradients were centrifuged at 156,000xg for 16 hours at 4°C in using an Optima Max-XP Ultracentrifuge. After 1 mL of the top layer was removed and 12 fractions of 250 μl were collected sequentially and numbered 1-12 from top to bottom. The different fractions were weighted determine density and used for western blot analysis and miRNA quantification.

For western blot analysis, 30 μl of each fraction was lysed in RIPA buffer with protease inhibitors (Sigma Aldrich). Protein concentrations were determined using Pierce BCA protein assay (Thermo Fisher) and equal amounts were loaded and resolved on 10% SDS-PAGE gel (Thermo Fisher). After transfer onto nitrocellulose membranes, samples were probed for GFP (Thermo Fisher, A-11122, 1:1000). ECL Anti-Rabbit IgG (Sigma) was used as secondary antibody corresponding to the primary antibody. The remaining volumes were used for RNA isolation and miRNA RT-qPCR quantification.

Intracranial Tumor Injection

Adult miR-21 null mice were first anesthetized using 2.5% isoflurane in 100% oxygen via a nose cone. The left striatum was then either injected with 1×10^5 cells of GL261.palmGFP.H2B.mRFP (GL261.pGHR) suspended in 2 μL OptiMEM or OptiMEM alone. Using a stereotactic frame, the cells were implanted at three coordinates from bregma: 0.5 mm left, 2 mm anterior and a depth of 2.5 mm from the skull. Three weeks after implantation, the mice were anesthetized with 120 μL of a mixture of ketamine (17.5 mg/ml) and xylazine (2.5 mg/ml) followed by transcardial perfusion with 50 mL cold Dulbecco's phosphate-buffered saline (DPBS) without magnesium and calcium for subsequent FACS using a perfusion pump (Minipump Variable Flow, Fisher Scientific).

Tissue Digestion

Neural Tissue Dissociation Kit (P) (Miltenyi Biotec) was used to process the brain into a single cell suspension. Brains were placed into a GentleMacs C-tube (Miltenyi Biotec) with 1.9 mL Buffer X with 50 μl Neural Buffer P. Brain was dissociated using the gentleMACS Dissociator (Miltenyi Biotec) on the brain program settings, according to manufacturer's protocol. Myelin removal was achieved using magnetic separation together with anti-myelin beads (Miltenyi Biotec). The final cell suspension was re-suspended in 1X DPBS without calcium (Ca^{2+}) or magnesium (Mg^{2+}) (Corning) supplemented with 2 mM EDTA (Thermo Fisher) and 0.5% BSA (Sigma) following cell staining and FACS.

Flow Cytometry Preparation

Non-specific binding of the immunoglobulin to the Fc receptors was blocked by incubating cells 10 min on ice in 0.5% BSA in DPBS (without Ca^{2+} or Mg^{2+}) with 2 mM EDTA supplemented with TruStain fcX (anti-mouse Cd16/32, BioLegend, #101319, clone 93, 1:100). Cells were stained with anti-CD11B-Alexa647 (clone M1/70, 1:100) and anti-CD45-PE-Cy7 (clone 30-F11, 1:100) for 30 min on ice. Finally, cells were washed with 1 mL DPBS (without Ca^{2+} or Mg^{2+}) with 0.5% BSA and 2 mM EDTA and were centrifuged at 300 × g for 10 min, resuspended in 0.5% BSA, 2 mM EDTA in DPBS (without Ca^{2+} or Mg^{2+}) and passed through a 35 μm nylon mesh strainer (BD Falcon). DAPI was added to cells at final concentration of 1 μg/ml. Live cells were sorted using a BD FACSAria II SORP Cell Sorter. Sorted cells were directly lysed in RLT Plus buffer (QIAGEN) and RNA was extracted using the RNeasy Plus RNA isolation kit (QIAGEN) according to manufactures protocol following appendix D.

Image Stream Analysis

Following protocol described above to dissociate cells from the whole brain, cells were stained as listed above with anti-CD11B-PE (clone M1/70, 1:100) and anti-CD45-PE-Cy7. After staining, cells were fixed and permeabilized with BD Cytofix/Cytoperm following manufacturing protocol. After fixation and permeabilization cells were stained with anti-GFP-Alexa Fluor 647 (clone FM264G, 1:100) and DAPI to a final concentration of 1μg/ml. Flow imaging was done using Amnis ImageStream mkII Imaging Flow Cytometer.

Intracranial Injection of EVs

Isolation of EV was done from conditioned media after 48 hours of culturing GL261 in RPMI with 1% P/S and 5% EV-depleted FBS (see "Cell Culture"). The differential ultracentrifugation protocol consisted of subsequent centrifugation at 300xg for 10 min and

2000xg 10 min. Supernatants were filtered through 0.8μm filter (Sigma) and centrifuged for 100,000xg (*k*-factor of 220.1) 120 min in Quick-Seal® Polypropylene Tubes (Beckman) using Type 70 Ti in Optima XE ultracentrifuge (Beckman) to pellet EVs. To wash and concentrate EVs, pellets were resuspended in remaining supernatant supplemented with OptiMEM and concentrated by centrifugation at 100,000xg (*k*-factor of 190.7) for 120 min in Thinwall Polypropylene Tubes (Beckman) using MLS-50 Swinging-Bucket Rotor (Beckman) in an Optima Max-XP Ultracentrifuge. Final EV pellet was resuspended in DPBS and characterization of EVs was performed by size distribution analysis using nanoparticle-tracking analysis (NTA 3.2; Malvern), with screen gain set at 3.0 and camera level at 13.0.

Following procedures as described in intracranial tumor implantation method section EVs or an equal volume of carrier fluid (PBS) was injected intracranially. Microglia were isolated 16 and 40 hours after injection of EVs or DPBS following procedures, as previously described.

RT-qPCR

cDNAs for gene expression analysis with RT-qPCR were prepared using the SuperScript VILO cDNA Synthesis Kit (Invitrogen). qPCR mix was prepared following manufacturing protocol of Power SYBR Green PCR Master Mix (Applied Biosystems). qPCR was performed using the QuantStudio 3 PCR system (Applied Biosystems). The cycling conditions used were 50°C for 2 min, 95°C for 10 min, and 40 cycles of 95°C for 15 s and 60°C for 1 min following dissociation analysis. All qPCR reactions were done in triplicate and normalized to *β-Actin* mRNA levels.

miRNA expression analysis was performed using miRCURY LNA miRNA PCR kit following manufacturing's protocol. miRNA expression was normalized to *U6* or UniSP6 spike-in RNA as listed in figure legends.

Digital Droplet PCR (ddPCR)

To evaluate gene expression of from cells isolated after intracranial injection of EVs, cDNA was prepared using the SuperScript VILO cDNA Synthesis Kit (Invitrogen). Gene expression was analyzed using ddPCR following PrimePCR ddPCR Gene Expression Probe Assay. Using protocol as listed by manufacturer droplets were generated with DG8 Cartridge using QX200 droplet generator (Bio-Rad) and PCR performed with thermal cycling conditions as described. QX200 Droplet Reader and QuantaSoft Software (Bio-Rad) were used to analyze the gene expression.

RNA Sequencing

The RNA concentration and integrity (RIN score) were determined using the Agilent 2100 Bioanalyzer Pico-chips (Agilent Technologies) following manufacturing protocol. RNA libraries were prepared with poly(A) selection using 3′-SMART CDS Primer II A within the SMARTer Ultra Low Input RNA Kit for Sequencing–v3 (Clontech Takara) following manufacturer's protocol including ERCC RNA Spike-In Mix (Life Technologies). Following first strand synthesis, cDNA was purified with 1x Agencourt AMPure XP beads (Beckman Coulter), as described in SMARTer protocol. Nextera® XT DNA Library Preparation kit (Illumina) was used for sample barcoding and fragmentation according to the manufacturer's protocol. Library amplification and library barcoding were achieved within 12 cycles of PCR. Subsequent PCR products were purified with 1.8x Agencourt AMPure XP beads according Nextera XT protocol. Library quantification was done using the SYBR® FAST Universal qPCR Kit (KAPA Biosystems). Equal molar individual libraries were pooled, and the pool concentration was determined using the KAPA SYBR® FAST Universal qPCR Kit. Finally, libraries were diluted and denatured with the addition of 1% PhiX Sequencing Control V3 (Illumina). 75-bp paired-end reads were generated using NextSeq 500/550 High Output v2 kit (150 cycles) on an Illumina NextSeq (Illumina).

QUANTIFICATION AND STATISTICAL ANALYSIS

Data Processing and Analysis

Raw sequencing data were processed by aligning to the mm10 genome using the STAR v2.4.0h aligner, and removing duplicate using the MarkDuplicates (picard-tools-1.8.4). Read counts were generated with Gencode's GRCm38.p3 GTF annotations as reference using htseq-count.

After aligning and read counting, the downstream analysis was performed using the DESeq2 (version 1.10) (Love et al., 2014) in R (version 3.2.3). Differential expression analysis as performed in DESeq2 was subjected to statistical significance using Benjamini and Hochberg multiple testing adjusted p values. The regularized logarithm (rlog) values were used for unsupervised clustering of top 750 most differential expressed genes between samples and to plot heatmaps using the gplots (version 2.17) heatmap.2 function in R.

Pathway analysis was performed in MetaCore using differential expression values between EV-GFP^{pos} versus EV-GFP^{neg} as generated in DESeq2. A cut-off value of significance of multiple testing adjusted p value < 0.05 was used to include differentially expressed genes.

Bar graph and MA plots were generated in GraphPad Prism (version 7.0c). Error bars display mean ± standard error of the mean (SEM). Significance was calculated using unpaired t test, multiple t tests and One-way ANOVA with Tukey's multiple comparisons test, with statistical significance defined as $p < 0.05$.

DATA AND CODE AVAILABILITY

Raw and processed transcriptomic data described in this manuscript are deposited in NCBI's Gene Expression Omnibus (GEO) and are accessible using GEO Series accession number GSE12607 at https://www.ncbi.nlm.nih.gov/geo/query/acc.cgi?acc=GSE126073.

All R scripts written for data processing are available online in a git repository. The files and information can be accessed at: https://github.com/slnmaas/miR21-Project.